Fluorescent pH sensor for heart monitoring

Master Thesis

Robbert Friendwijk

Delft University of Technology

TU Delft

Fluorescent pH sensor for heart monitoring

by

Robbert Friendwijk

to obtain the degree of Master of Science
at the Delft University of Technology,
to be defended publicly on Friday July 12, 2024 at 14:00

Student number: 4567331
Project duration: September 1, 2023 – July 12, 2024
Thesis committee:

Prof. dr. P. J. French,	TU Delft, supervisor
Dr. G. de Graaf,	TU Delft, supervisor
Dr. M. Mastrangeli,	TU Delft

TU Delft

Preface

Robbert Friendwijk
Delft, July 2024

This thesis was written as part of the Master of Electrical Engineering with the track Microelectronics at the Laboratory of Bioelectronics.
The goal of this thesis was to design a prototype sensor which was able to monitor heart tissue during cardiac surgery. During this thesis I found out that the bottle neck for this design was not so much in the electrical domain but more in the chemical domain. This posed somewhat of a challenge for me since I am an electrical engineer and have not been in contact with chemistry since high school. Nevertheless, I can say that I am proud of the end result. However, I could not have done this without the help of the following people, who I like to give my thanks.

First, I would like to thank my supervisors Paddy French and Ger de Graaf for their guidance through this thesis project.

I also would like to thank Robert Verhoeven from EKL, who was my supervisor in the chemical room in EKL. He helped me a lot with the production of the sensor layers and other lab related issues.

Furthermore, I would like to thank Hitham Amin, who helped me with my gaps in my chemical knowledge.

I also would like to thank Avik Sett, for his help during the measurements and for being my sparring partner during the last part of my thesis project.

Last but not least, I would like to thank my family and my girlfriend Julie for their continued support throughout my thesis project.

Summary

During most cardiac surgeries, a Cardiopulmonary bypass (CPD) is used. This is a machine which takes over the respiration and circulation functions of the heart during surgery. However, the blood supply to the heart and thus the supply of oxygen and nutrients, will be cut off when this occurs. This is also known as myocardial ischemia, which can lead to damage to the heart tissue and could even be fatal. Therefore, it is of paramount importance to detect ischemia before it causes irreversible damage.

There are several parameters that can indicate ischemia, including pH, oxygen and lactate. This work focuses on measuring the pH level of the heart tissue, since this could be measured noninvasively and is relatively simple. In order to get a clear picture of the consequences of ischemia throughout the heart, the pH level should be measured at different locations. To achieve this an optical fluorescence sensor is designed. This sensor consists of a sensor layer, two LEDs and an optical fibre connected to a spectrometer.

The fluorescent indicator dye used in the sensor layer is 8-Hydroxypyrene-1,3,6-trisulfonic acid trisodium salt (HPTS). This fluorescent dye has two excitation peaks, one at 405nm and one at 470nm and two emission peaks one at 440nm and one at 515nm. These different excitation and emission bands enable ratiometric sensing which improves accuracy and sensitivity. This is due to the fact that the intensity of the fluorescent emission at 515nm is directly proportional with the pH level, where the intensity of the fluorescent emission at 440nm is inversely proportional to the pH level. By taking the ratios of these measured intensities the pH can be determined.

The indicator dye is immobilized in a hydrogel which is thereafter deposited on a thin glass slide. This slide is placed above two LEDs which are matched with the excitation peaks of HPTS. Adjacent to the LEDs an optical fibre is placed to capture the fluorescent emission and direct it to the spectrometer which is connected to a computer. The designed sensor system shows a 5 fold increase in ratio of intensities over a pH range of 6.2-8.2, with a significant improvement in response time compared to other HPTS and hydrogel based pH sensors reported in literature.

Contents

1

Introduction

According to the NHLBI (National Heart Long and Blood Institute) over 2 million people each year around the world undergo cardiac surgery in order to solve various health problems [1]. The mortality rate of all the combined cardio surgical procedures is between 3-6% [2]. During most cardio surgical operations a Cardiopulmonary bypass (CPB) is used. A CPB takes over the functions of the heart and the respiratory system alongside temperature management, in order to maintain systemic perfusion during cardiac surgery [3]. However, the blood supply to the heart and thus the supply of oxygen and nutrients, will be cut off when this occurs. This is also known as myocardial ischemia, which can lead to damage to the heart tissue and could even be fatal [4]. According to Fan et al. [5], myocardial damage is one of the most common causes of morbidity and mortality after heart surgery. One of the most common methods of preventing the negative consequences of ischemia from happening, is the use of cardioplegia. Cardioplegia means, literally speaking, the artificial diastolic cardiac arrest. By arresting the heart, the energy demand of the heart tissue can be decreased with a factor of hundred [6]. This means that the heart can be in ischemic conditions for a prolonged time with decreased risk of irreversible damage. Therefore, it is important that the cardioplegic solution is distributed uniformly through the heart tissue. However, this can be impaired by anatomic and/or functional conditions [7]. These impairments include coronary stenosis and aortic regurgitation [5]. This would mean that in some parts of the heart tissue, the negative consequences of ischemia would occur earlier than would be expected. Therefore, it is of paramount importance to detect the negative consequences of ischemia as soon as possible to be able to counteract them.

It has been shown in multiple works that the pH level of the heart tissue is a clear indicator of the extent of ischemic stress [8], [9], [10]. This is mostly due to the changed metabolic processes in the heart tissue during ischemia. In this thesis a non invasive fluorescence sensor system is designed with the objective to monitor the heart during the cardiac surgery and to detect changes in the health status of the heart tissue. In order to achieve this objective, the following research questions will be answered.

RQ1: What are the key principles of fluorescence sensing and how can they be used for measuring acidity of heart tissue?

RQ2: What kind of materials are needed to produce the sensor?

RQ3: How should the optical system be designed to ensure accurate measurement results and simplicity?

In order to answer these research questions the thesis is outlined as follows. In the next section the medical background of myocardial ischemia and the relation with the acidity of the tissue will be discussed in more detail. Thereafter, the relation between the optical measurement methods will be discussed, in particular fluorescence sensing. Subsequently, the basic components of the optical system will be explained. In Chapter 2, the design choices made for the sensor system will be motivated and explained. In Chapter 3, the materials and methods used for the experiments will be discussed. Thereafter, in Chapter 4, the results are shown. Lastly, in Chapter 5 these results will be discussed and explained.

1.1. Medical Background

In this chapter the medical background of cardiac surgery and the causes and consequences of myocardial ischemia will be discussed.

Cardiac surgery is the speciality of medicine which is concerned with performing surgical treatment of the heart [11]. There are several types of cardiac surgeries. However, in this thesis we will be discussing open heart surgeries as opposed to minimally invasive surgeries. Open heart surgery is the traditional method to access the heart by opening the thorax [11]. During most open heart surgeries a cardiopulmonary bypass (CPB) is required. Sarkar et al. [3], defined CPB as: "A form of extracorporeal circulation whose function is circulatory and respiratory support along with temperature management to facilitate surgery on the heart and great vessels". In other words CPB takes over the functions of the heart and the respiratory system to maintain systemic blood flow during cardiac surgery. However, when CPB is used myocardial ischemia will occur. In order to understand why this is the case, the principle of myocardial ischemia will be explained.

Myocardial ischemia will occur when the blood flow to the heart tissue is halted [12]. This results in a loss of oxygen and nutrients supply. This will rapidly cause problems in the metabolism of the myocardium. When the oxygen supply to the myocardium becomes limited the cells switch from aerobic to anaerobic metabolism [13]. This has a significant influence on the production of Adenosine triphosphate (ATP), which are molecules that can be seen as the chemical fuel which provides energy for intracellular processes [14]. Normally during aerobic metabolism about 97% of the ATP formed in the heart is generated by the oxidation of fatty acids and pyruvate in the mitochondria [15]. Around 60% of this ATP is used for the cardiomyocyte contractile function. The rest is used for the ion pumps which among other things make diastolic relaxation possible [15]. When the metabolism changes form aerobic to anaerobic due to ischemia, the ATP production efficiency decreases significantly. One glucose molecule produces 2 ATP molecules during anaerobic conditions as opposed to 36 in aerobic conditions. Due to this change in cellular metabolism, the pyruvate is broken down into lactate and residual protons which lead to a lower intracellular pH level. This change in pH level is what will be the focus on in this thesis, since this is what will be measured. However, in order to understand the detrimental effects of myocardial ischemia, the cascading events resulting from this change in pH have to be discussed further.

Due to the excess protons, the Na^+-H^+ ion gate is activated which leads to an efflux of H^+ and an influx of Na^+ ions [16], see Figure 1.1. This leads to an increase in the Na^+ concentration in the cytosol. Due to this increase the Na^+-Ca^{2+} ion gate is activated which transports the accumulated Na^+ out of the cell and Ca^{2+} into the cell. Moreover, due to the decrease in ATP in the cell which is the result of the switch between metabolism pathways, the activity of the active ion pumps is inhibited. Therefore, the pumps which normally pump Na^+ out of the cell and K^+ into the cell in order to maintain homeostasis, will no longer function. This leads to an even higher Na^+ concentration. The increased concentration of Na^+ and Ca^{2+} leads to inhibited repolarization and therefore leads to suppressed myofibril contracture. Furthermore, high Ca^{2+} levels leads to the activation of certain enzymes which are related to reactive oxygen species (ROS), lipid peroxidation, cell function loss and ultimately cell death [16].

As can be read above myocardial ischemia itself can already do significant damage to the myocardium. However, there is also another mechanism which is related to myocardial ischemia which also causes cell damage. This phenomenon is called myocardial reperfusion injury. Upon reperfusion the oxygen supply to the myocardium is restored. This results in a restoration of the pH level by washing out the lactic acid and transporting H^+ out of the cell. Furthermore, due to the sudden inflow of oxygen, reactive oxygen species (ROS) are created [17]. These free radicals damage the sarcolemma which in turn contributes to a intracellular Ca^{2+} overload. This intracellular Ca^{2+} overload in combination with the restored pH level make the mitochondrial permeability transition pore (mPTP) open which leads among other things to the release of Cytochrome c which is in turn responsible for apoptosis [18].

One of the most common measures to prevent the previously mentioned consequences of cardiac surgery, is cardioplegia. This is a pharmacological substance that can be administered to the patient in order to arrest the heart [20]. The main component of the most used cardioplegic solutions are

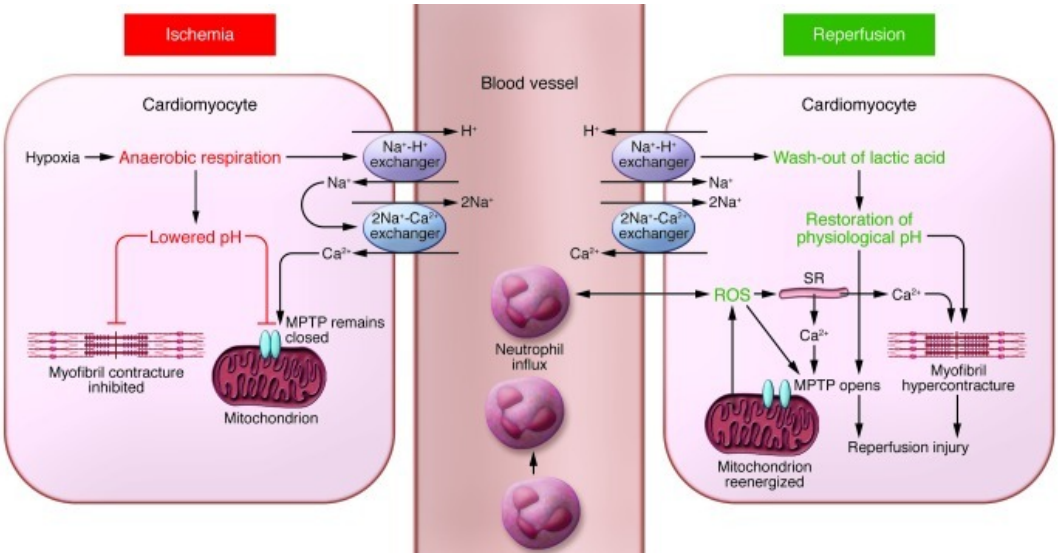

Figure 1.1: Schematic representation of the cascade of reactions following myocardial ischemia: When ischemia occurs the myocardial cells will switch from aerobic to anaerobic metobolism due to the lack of oxygen. This will result in an accumulation of lactate and a decreased pH level. This triggers Na^+-H^+ ion gate to start working which leads to the influx of Na^+ which in turn triggers the influx of Ca^{2+}. The acidic conditions and the overload of intracellular Na^+ and Ca^{2+} prevents repolarization and thus myofibril contracture. Furthermore high Ca^{2+} levels leads to the activation of certain enzymes which are related to reactive oxygen species (ROS), lipid peroxidation, cell function loss and ultimately cell death [16]. Upon reperfusion the H^+ is flushed out of the side to restore physiological pH. This results in an even larger Ca^{2+} overload and results in combination with the ROS to the opening of the MPTP pore which can lead to cell death. Figure is reprinted from [19]

potassium ions, which will induce hyperkalemia [21]. Hyperkalemia indicates a potassium concentration higher than normal. The normal resting membrane potential of cardiomyocytes is around -85mV [22]. However, when the potassium concentration will increase, this membrane potential will increase as well and become less negative. When the resting potential is increased to -65mV it will no longer pass action potentials and diastolic arrest is initiated. By inducing this arrest the metabolic processes of the cardiomyocytes are slowed down which means less oxygen and other nutrients are needed. This means that the effects of myocardial ischemia and reperfusion injury will be reduced. Another reason why surgeons apply cardioplegic solutions for cardiac surgery is that it will also provide a motionless surgical field.

However, according to the results obtained in [7], not in all cases cardioplegia is distributed uniformly through the whole heart. This would mean that in some heart cells the metabolic processes are not halted and ischemia will occur at an increased rate. For this purpose, it would be convenient to monitor the tissue to detect the onset of ischemia before it can do permanent damage. There are several indicators for ischemia, such as lactate concentration, oxygen concentration, carbon dioxide concentration and pH level. In this research the focus will be on monitoring the pH-level. How this will be achieved will be discussed in the next section.

1.2. Fluorescence

In order to understand the design of the pH sensor, first the basic principles of fluorescence must be explained. These principles will be mostly derived from the books Molecular Fluorescence [23] and Principles of Fluorescence Spectroscopy [24].

Fluorescence is defined as the emission of visible light due to the absorption of photons. When a photon of sufficient energy is absorbed by a fluorescent material, it can promote the electrons in this material from a lower energy level (ground state) to an higher energy level (excited state). Typically electron pairs reside in the singlet state when in the ground state (denoted by S_0). In this state, electron pairs possess opposite spins, resulting in a spin quantum number S equal to zero as can be seen from Equation 1.1, where $s_i = \pm\frac{1}{2}$. Therefore, the multiplicity of states, given by Equation 1.2, is one. This

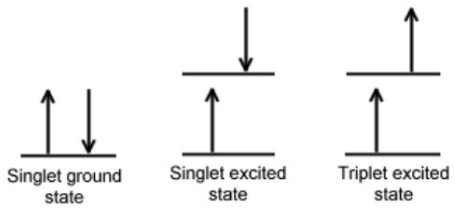

Figure 1.2: Visual representation of the singlet and triplet state reprinted from [25]

is why this state is called the singlet state. The visual representation of the singlet and triplet state can be seen in Figure 1.2. Upon excitation one of the electrons can be excited to a higher energy level. When the electrons keep opposite spins during this transition they will be in the excited singlet state, typically denoted by S_1, S_2 and so forth.

$$S = \sum s_i \tag{1.1}$$

$$M = 2S + 1 \tag{1.2}$$

After excitation de-excitation will occur. This can happen through different pathways.

The first pathway that will be discussed is internal conversion. This is a non radiative transition between energy states with the same spin multiplicity and typically occurs in higher energy states [23]. For example when an electron is excited to an energy state higher than S_1, so to S_2 or S_3, internal conversion will take place. The electric energy is converted to vibrational energy. Which is thereafter typically dissipated as heat to the surrounding environment.

which will temporarily heat up the material, the excess energy is dissipated and the electron will be relaxed to the zero vibrational level of the state of S_1. This all happens in a timespan of 10^{-13} - 10^{-11}s. Due to the fact that this process does not involve the emission of a photon, it is called a non radiative transition.

The most important de-excitation pathway is that of fluorescence. This is typically the transition from the S_1 to the S_0 state accompanied by the emission of a photon. The wavelength of this photon it typically higher than that of the excitation wavelength. This is mostly due to the energy losses that occurs due to internal conversion which is described before. This difference between the excitation wavelength and the emission wavelength is also known as the Stokes shift. The Stokes shift is a fluorescent material property and will be discussed in the next section. Another aspect that connects internal conversion to the fluorescent emission is Kasha's rule. This rule states that the emission wavelength of a fluorophore is independent on the excitation wavelength. This is due to fact before fluorescence can take place the internal conversion has occurred. Therefore, the electrons will almost always be in S_1 prior to relaxation to S_0. The energy difference between these states is a material property and thus will be the same for different excitation wavelengths, which means that the emission wavelengths will also be the same for the same material.

Another de-excitation pathway is intersystem crossing. This happens when an excited electron changes it spin, which then results in electron pair with parallel spins. From Equations 1.1 and 1.2 it can be seen that this results to a spin quantum number of one which means the multiplicity of states becomes three. Therefore, this state is called the triplet state. The probability of intersystem crossing is dependent on the singlet and triplet states and is therefore a material property. The difference between the spin configuration of the singlet and triplet state causes the triplet state to have a lower energy level than the singlet state. From the triplet state T_1, an electron can de-excite to S_0 accompanied by the emission of a photon. However, due to the difference in multiplicity of states this process occurs at a significantly lower rate. This means that the effect of phosphorescence can be observed for seconds or even minutes.

1.2.1. Fluorescent material properties

In this section the material properties that attribute to fluorescence along with their relevance to fluorescent sensing will be discussed.

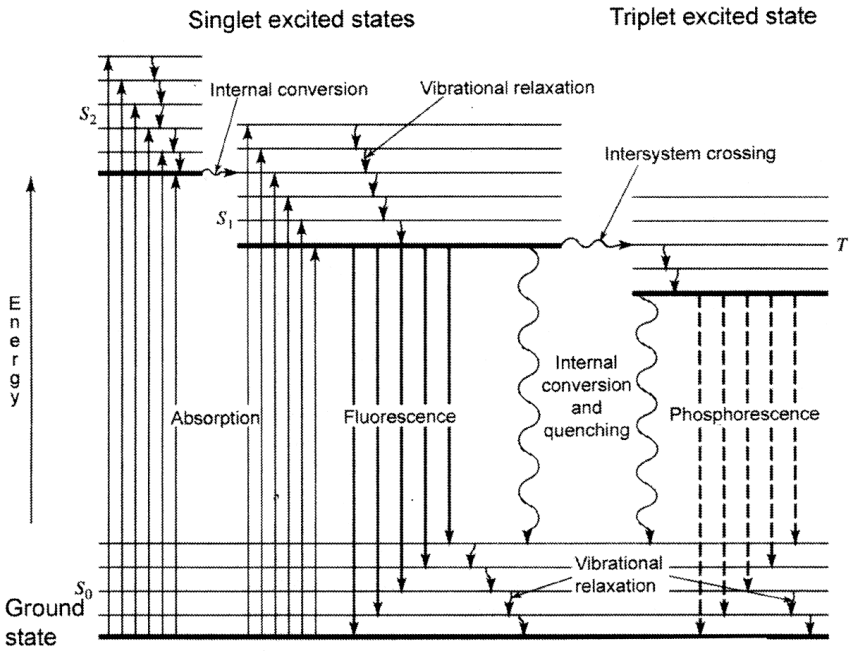

Figure 1.3: Jablonski diagram from reprinted from [26]

Stokes shift

As said in the previous section, one of the consequences of internal conversion which leads to vibrational relaxation is the Stokes shift. The Stokes shift is the difference in energy between the absorption band maxima and the lower energy emission. This lower energy emission can be observed to be red shifted and thus has a longer wavelength. The difference in energy is due to the energy loss during the excitation state of the electrons. The principle of the stokes shift makes fluorescence useful for sensor applications, since because of the stokes shift distinction can be made between the excitation light and the fluorescent emission light. This drastically increases the sensitivity of the sensor.

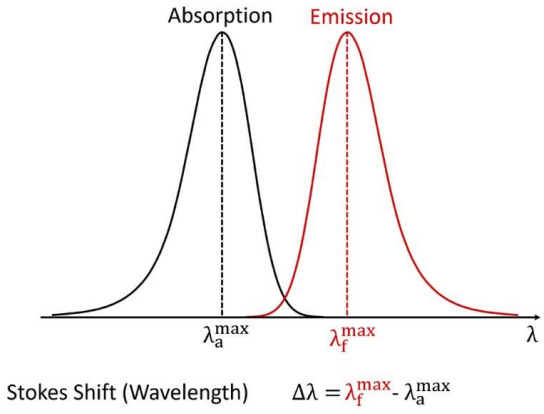

Figure 1.4: Visual representation of the stokes shift which is the difference between the wavelength of the emission peak and the wavelength of the absorption peak. Reprinted from [27]

Quantum yield

Another important characteristic of a fluorophore is the quantum yield. This is the ratio between the absorbed photons and the emitted photons. The quantum yield is commonly expressed in rate constants of radiative and non radiative decay which are denoted as k_r and k_{nr} respectively in Equation 1.3. The rate constants are the first derivative of the exited electron concentration of the material. Note that there are multiple non radiative processes that have influence on the quantum yield. As can be

seen from the Equation, the quantum yield can approach unity when k_r » k_{nr}, which is the case for strong fluorophores.

$$\Phi = \frac{k_r}{k_r + \Sigma k_{nr}} \tag{1.3}$$

Fluorescent life time

The fluorescent life time of a fluorophore indicates the time electrons spend on average in the exited state before it returns to the ground state. The expression for the fluorescent life time is shown in Equation 1.4. As can be seen from the equation the lifetime is directly related to the quantum yield. The lifetime of a fluorophore can be influenced by multiple material properties like the chemical structure, molecular environment and the fluorophore concentration. Another influence on the fluorescent life time of a fluorophore is the pH of the environment. This is utilized in pH sensor which are based on the lifetime of fluorophores. This dependence will be discussed in more detail in the next section.

$$\tau = \frac{1}{k_r + \Sigma k_{nr}} \tag{1.4}$$

Quenching

Fluorescence quenching is defined by the IUPAC goldbook to be: "Deactivation of an excited molecular entity intermolecularly by an external environmental influence (such as a quencher) or intramolecularly by a substituent through a non-radiative process" [28]. What is meant by this is that quenching decreases the fluorescence intensity due to interactions with other molecules also known as quenchers. A distinction can be made between static and dynamic quenching.

Static quenching occurs when a fluorophores forms a complex with an quenching molecule in de ground state. When such a complex is excited it will quickly return to the ground state without the emission of a photon.

Dynamic quenching occurs when the fluorophore is in the excited state. When such a molecule interacts with a quencher it will transfer its energy to the quencher and will return to the ground state without the . emission of a photon. It should be noted that the structure of the molecules themselves are not chemically altered in this process as opposed to static quenching. The decrease of intensity due dynamic quenching is described in the Stern-Volmer Equation 1.5 , where F and F_0 are the fluorescence intensities with and without the quencher present respectively and K_{sv} is the Stern-Volmer constant which is the product of the quenching rate constant k_q and τ_0, the fluorescence life time of the fluorophore when the quencher is not present. Lastly, $[Q]$ denotes the concentration of the quencher [24].

$$\frac{F_0}{F} = 1 + K_{sv}[Q] = 1 + k_q \tau_0 [Q] \tag{1.5}$$

Another cause of quenching is photoinduced electron transfer (PET). When certain fluorophores absorb light it can change its redox properties which might enable photoinduced electron transfer [29]. This occurs when an excited donor molecule D transfers an electron to an acceptor molecule A or vice versa, which results in charged ion pair which relaxes to the ground state and non radiative dissipation of excited state energy. The Rehm-Weller equation1.6 is used to predict the efficiency of the photoinduced electron transfer and to determine whether the donor and acceptor pairs are suitable for the transfer. In this equation the Gibbs free energy change (ΔG)is calculated which represents the driving force behind the photoinduced electron transfer [30]. This means that the more negative ΔG becomes the more likely PET will occur. In Equation 1.6, the oxidation potential of the donor and the reduction potential of the acceptor are indicated by $E(D/D^*)$ and $E(A/A^*)$ respectively. The term ΔG_{00} represents the energy that is needed for the S_0 to S_1 transition. The last term describes the coulombic attraction energy between the donor and acceptor ions.

$$\Delta G = E(D/D^*) - E(A/A^*) - \Delta G_{00} - \frac{e^2}{\epsilon d} \tag{1.6}$$

From Equation 1.6, it can be seen that careful matching of the fluorophore and the quencher is needed to enable PET. In [31], several applications of PET are are shown. These include a case were

a fluorophore and a quencher are matched for PET which results in Fluorescence quenching. However, when the the pH of the environment decreases and the fluorophore is protonated, it will increase the oxidation potential. This will result in a inhibition of PET and thus in an increase of fluorescence emission.

1.3. Relation pH and fluorescence

In the previous section some of the basic characteristics of fluorescent materials are discussed. In this section the relation between those characteristics and the pH will be explained.
In order to understand how pH can be measured using fluorescent materials first the definition of pH has to be briefly revisited. pH refers the acidity of an aqueous solution. It is defined as the negative logarithm of the activity of Hydrogen ions which is in most cases a good approximation of the concentration of hydrogen ions, see Equation 1.7.

$$pH = -log(a_{H^+}) \approx -log[H^+] \tag{1.7}$$

However, in most fluorescent measurements techniques not the activity of hydrogen atoms are measured, but the concentration of protonated (A) of deprotonated (B) forms of the fluorescent indicator, see Equation 1.8. In this equation the protonated concentration (A) of the fluorescent indicator represents the concentration of indicator molecules that has gained a hyrdogen atom (H^+). This indicates that the indicator molecule is in an acidic environment. The depronated concentration (B) of the indicator dye represents the concentration of indicator molecules that has lost a proton which indicates that the molecule is in a basic environment. The term pK_a is the acid dissociation constant and denotes the equilibrium point of the acid or base. This means that if the solution has a pH value of pK_a then no reactions will take place.

$$pH = pK_a + log\frac{[A]}{[B]} \tag{1.8}$$

The change in protonation state of an indicator molecule influences the electronic structure of the material. This means for that the addition or subtraction of a Hydrogen atom can alter the position of the energy levels within the molecule. This results in a shift in the absorption and emission spectrum of the fluorophore. Furthermore, the quantum yield can also be influenced by changes of pH. This is due to the fact that protonation can influence the rate of radiative or non radiative relaxation.
These relations between the pH and the characteristics of a fluorophore are utilized by various fluorescence measurement techniques. These different techniques will be discussed in the next section.

1.4. Fluorescence measurement techniques

In this section the three most used techniques to measure pH by using fluorescence will be discussed. These different measurement methods are described in detail by Steinegger et al. [32] and Valeur [23].

1.4.1. Fluorescence intensity sensing

One of the most widely used measurement techniques are based on the change in fluorescence intensity as function of pH. As described in Section 1.3, a change in pH can cause a change in the quantum yield and a shift in the emission spectrum of the fluorophore. In order to perform fluorescent intensity measurement the following elements are needed: constant illumination by light source, fluorescent material which changes its properties as a function of pH and an image capturing device. Due to the fact that a constant illuminating light source is used this kind of measurement is classified as a steady state measurement.

In the ideal case the fluorescent intensity would be solely dependent on the pH value of the environment. Unfortunately, this is not the case. In Equation 1.9, the formula for the intensity of a fluorescent material is shown. It can be seen that the fluorescence intensity (F) is dependent on the following aspects: The illumination intensity of the light source (I), the absorbance of the indicator base or acid (ϵ), the concentration of the fluorophore's acid or base form (c), the quantum yield (Φ) and a geometrical factor k which represents the geometrical alignment of the measurement instruments [32].

$$F = I \cdot \epsilon \cdot c \cdot l \cdot \Phi \cdot k \tag{1.9}$$

It can be concluded from Equation 1.9 that the fluorescence intensity is not a robust parameter, since it is influenced by a large number of factors. Therefore, when using this method for optical pH sensing careful calibration is needed in order to compensate for the other factors than the fluorophore's acid or base form. Another method to compensate for the other parameter is to make using of ratiometric measurements. In ratiometric fluorescence sensing instead of measuring the intensity at one wavelength, the ratio of fluorescence intensities of two wavelengths is taken. By using this method the influence of factors such as illumination intensity, detector sensitivity and geometry is minimized. Ratiometric measurements can be implemented in using two different methods. The first method makes use of two fluorophores in the same support matrix, one which is responsive to changes in pH and one who does not. Ratiometric measureent are made possible by taking the ratios of the intensities of fluorescence emission of both the dyes. However, special care must be taken in the selection of these dyes since it the emission of both fluorophores should be clearly distinguishable. Moreover, more complex optical systems are needed since most of the time excitation spectra of the two fluorophores are not the same. For example in [33], the use of pH responsive fluorophore diazaoxy-triangulenium (DAOTA) in combination with the pH insensitive fluorophore bis(2,6-diisopropylphenyl)terrylene diimide (TDI) was discussed. These dyes have different emission peaks so both have to be measured. Another method of ratiometric measurements is the use of fluorophores which have two excitation bands and/or two emission bands. This would mean that only one fluorophore is needed to be able to implement ratiometric sensing. Examples of such fluorophores include HPTS [34] and BCECF [35]. The disadvantage of using this kind of measurement methods is that a more complex measurement system is needed alongside a carefully chosen fluorophore which has two excitable wavelengths.

1.4.2. Fluorescence lifetime sensing

As discussed in the previous section the intensity of fluorescence emission decays over time when excited with an light pulse. This process happens in a very short time span, generally around 10 ns [24]. When a fluorophore is excited with a light pulse the intensity of the fluorescence after the termination of the light pulse can be given by Equation 1.10. In the equation I_0 denotes the fluorescence emission intenisity at the precice moment the light pulse is terminated. Furthermore, τ give is the fluorescence lifetime of the fluorophore, which is the average amount of time the fluorophore remains in the excited state. The principle of lifetime sensing is a change in decay time when the sensor is in the presence of the analyte, in this case pH changes. In other words fluorophores that are suitable for lifetime sensing have a different lifetime in their protonated form than that of the deprotonated form. These changes are mostly in the nanoseconds which can be measured in the time domain, by observing the lifetime after the excitation by a short light pulse or in the frequency domain were the excitation source is modulated [36]. The schemes for these two methods are shown in Figure 1.5. On the top of top of the figure an idealised case shown were the illumination source is a perfect pulse this then leads to an intensity decay with time constant τ. Of course in the real application an ideal pulse is not possible but when the pulse duration is significantly shorter than the lifetime of the fluorophore than it is a good approximation.

$$I(t) = I_0 e^{\frac{-t}{\tau}} \tag{1.10}$$

In the bottom of the figure the scheme for phase modulation sensing can be seen. In this case the excitation source is sinusoidal signal with a predetermined frequency. When this source is used to illuminate the fluorophore the fluorescence emission will have the same frequency but due to the decay times it will be phase shifted. This phase shift can thereafter, be measured. The advantages of lifetime sensing include: independence of probe concentration, detector sensitivity and low influence of photobleaching [37]. The disadvantage of lifetime sensing is the need or more sophisticated equipment when compared to for example fluorescence intensity sensing. This is due to the fact that the light source used should be able to make short enough pulses. Furthermore, the detector should be able to be gated with a high enough frequency in order to record the intensity decay with a high enough resolution. This all should be combined with a fluorophore with a large enough lifetime to be observable. A typical time domain life time sensing scheme can be seen in Figure 1.6. In the figure it can be be seen that for short period of time the light source is turned on. Thereafter, when it is turned off the detector will be turned on after a short period of time to make sure that all background fluorescence is decayed. Thereafter, it will make two recording at different time intervals. Then the life time can be calculated using Equation 1.11.

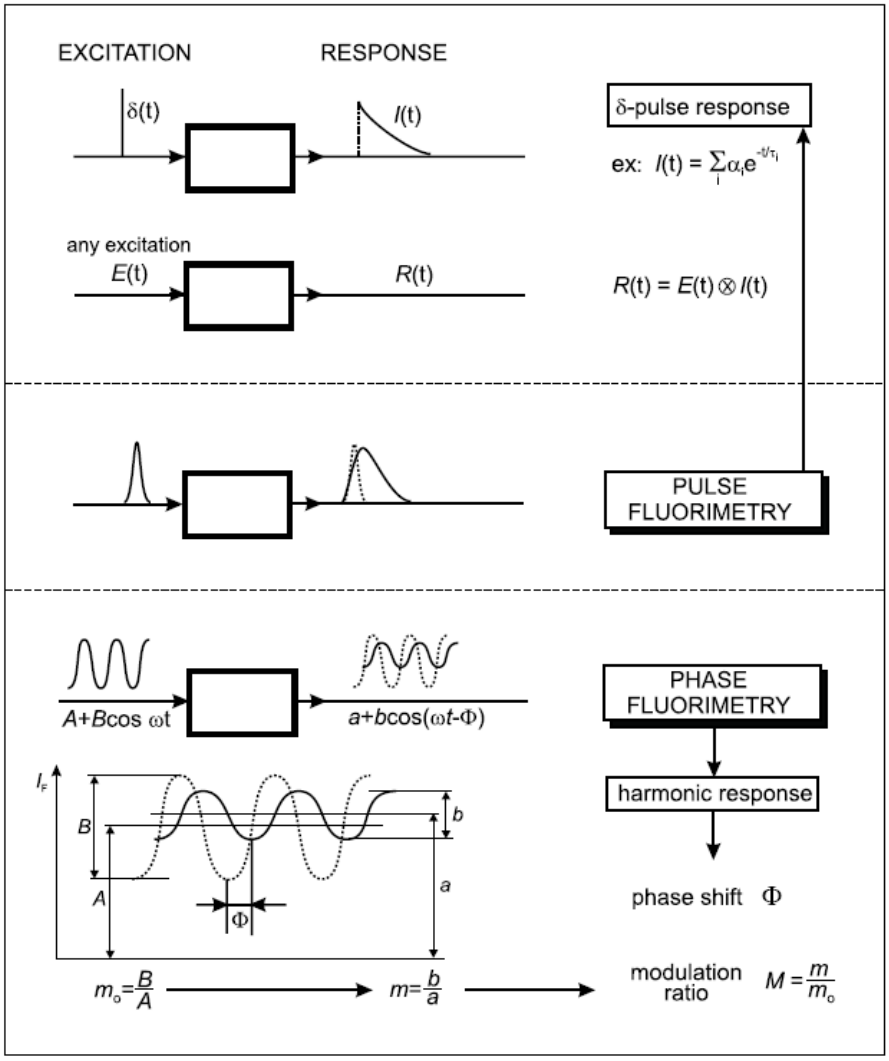

Figure 1.5: Fluorescence life time sensing schemes. Reprinted from [23]

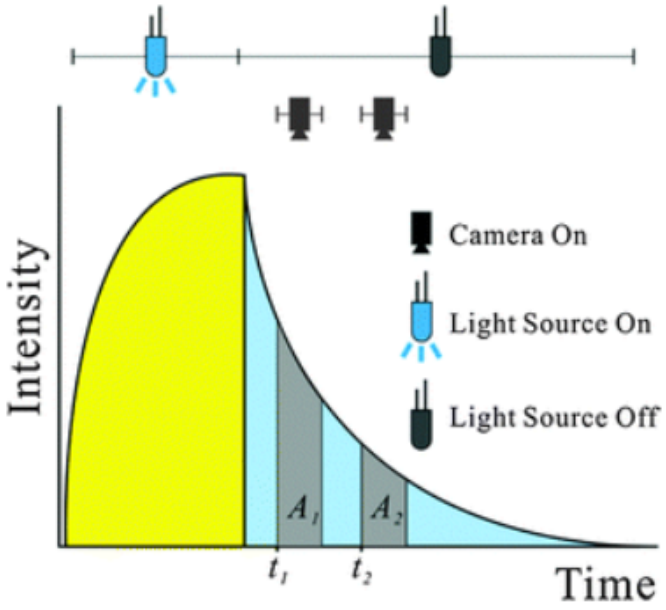

Figure 1.6: Time domain lifetime sensing scheme. Reprinted from [37]

$$\tau = \frac{t_2 - t1}{ln\frac{A_1}{A2}} \tag{1.11}$$

1.4.3. Förster resonance energy transfer (FRET)

Energy transfer is another phenomenon that can occur in fluorescent materials. It starts with a donor molecule in the excited state and an acceptor molecule in the ground state. Typically the wavelength of emitted photon of the donor molecule is longer than the absorbed photon, see 1.2.1. This wavelength can then overlap with the absorption spectrum of the acceptor molecule and thus can be absorbed by it and can emit a photon of a longer wavelength. This means that an energy transfer has occurred between the donor molecule and the acceptor molecule. The rate of the energy transfer is dependent on the following parameters: the amount of overlap between the emission spectrum of the donor and the absorbance spectrum of the acceptor, the distance between the donor and acceptor and the quantum yield of the donor. Therefore, the transfer rate $k_t(r)$ is defined as can be seen in Equation 1.12, where τ_d is the decay time of the donor molecule, r is the distance between the donor and acceptor molecule and R_0 is the Förster distance. The Förster distance defined as the distance where the efficiency of the resonance energy transfer is 50%. It depends on the spectra of the donor and acceptor molecules and their orientation.

$$k_t(r) = \frac{1}{\tau_d}\left(\frac{R_0}{r}\right)^6 \tag{1.12}$$

FRET can be used for pH sensing by making the donor or acceptor a pH dependent material. This means that the donor or acceptor would change its emission/absorption spectrum or its orientation as a function of pH. This change can thereafter be measured as the emission of the acceptor. The advantage of FRET is the sensitivity as can be seen in Equation 1.12 as it has a sixth order dependence on the Förster distance and the distance between the donor and acceptor. Furthermore, ratiometric measurements are possible due to the use of two different materials as donor and acceptor. However, this sensitivity for distance can also be disadvantage for pH sensing since for the sensor to operate accurately the initial distance between the donor and acceptor molecule have to be accurately defined. Furthermore, two different dyes are needed for a Förster sensor to work and careful selection is needed since the emission and absorption spectra have to overlap.

1.5. Indicator dyes

In the previous section the fluorescent material properties are discussed. In this section fluorescent pH indicators themselves will be outlined. First a general view of an fluorescent pH indicator will be given. Thereafter, several commonly used pH indicators will be discussed with their specifications, advantages and disadvantages.

In order to select the best fitting fluorescent pH indicator several aspects have to be taken into account. First of all the pH range of the fluorophore should be known. Mostly this is around the pKa of the material which gives the equilibrium point between the acidic and basic form of the fluorophore. This pKa is mostly dependent on the chemical structure of the fluorophore and the environment in which the fluorophore is submerged. Typically, single fluorophore sensors have a relatively small pH range of 2-3 pH units. However, this range can be increased by using two fluorophores in the same sensor as has been done in [38] and [39]. Thereafter, the excitation and emission spectra have to be considered. Each fluorophore has its own optimal excitation wavelength, therefore careful selection is needed to receive the maximum fluorescence intensity. The same can be said for the emission of the fluorophore. Since the wavelength of this emission should be in the detectable range of the photodetector used in the sensor system. Furthermore, the Stokes shift, see section 1.2.1, needs to be considered since this can determine the background noise in the fluorescent signal. Another parameter is the quantum yield and the sensitivity of the fluorophore since this determines the magnitude and difference in signal strength of your fluorophore. Lastly, the costs and manufacturing difficulty should be taken in to account to make sure that the overall sensor system does not become to costly and does not take to much time to manufacture. In the following subsections the most used fluorophores will be discussed.

1.5.1. Fluorescein

One of the most used fluorescent pH indicators is Fluorescein and its derivatives [40]. This popularity is mostly due to its high intensity fluorescence, reversible pH sensitivity, low cytotoxity and stability [41]. In Figure 1.7, the chemical structure of two fluorescein forms can be seen. These are the two forms in which fluorescein can be present in the pH range of 6-10 which is within the scope of this work. The pH dependent fluorescent properties are related to these two forms. This is due to the fact that by transitioning to a lower pH level the dianionic form is converted to the mono-anionic form. This can be observed in the fluorescent intensity of fluorescence since the dianionic form has quantum yield of 0.9 and the mono-anionic form has a quantum yield of 0.3 [42]. Therefore, a significant decrease in fluorescent emission can be observed when transitioning from a higher pH value to a lower pH value. This difference can be seen in the emission spectrum which is shown in Figure 1.8. Fluorscein has a maximum excitation intensity at a wavelength of 490nm and a maximum emission intensity at 512nm. From these two wavelengths it can be concluded that the stokes shift is relatively small. Therefore, care must be taken to separate the excitation and emission wavelengths. However, the most problematic disadvantage of using fluorescein is photobleaching. This means that its fluorescent intensity decreases over time. This would make the sensor unreliable when used for a longer period of time.

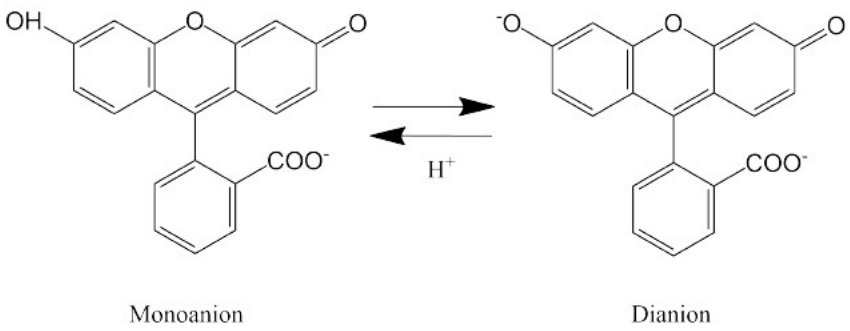

Figure 1.7: Fluorescein molecule proton interaction between the monoanion form and the dianion form [43]

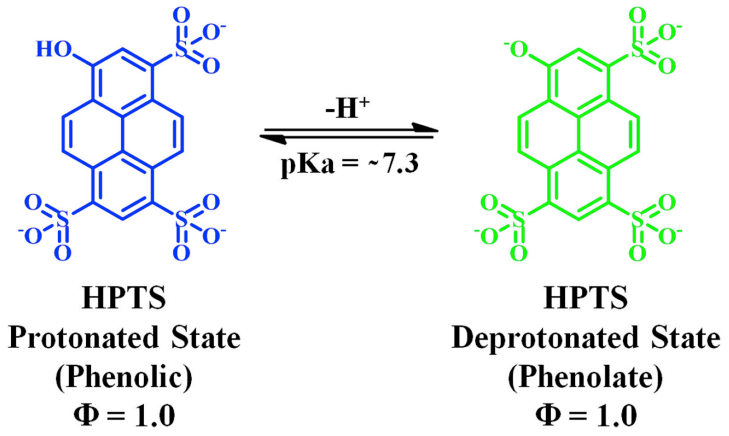

Figure 1.9: Molecular structure of HPTS in protonated and deprotonated form [46]

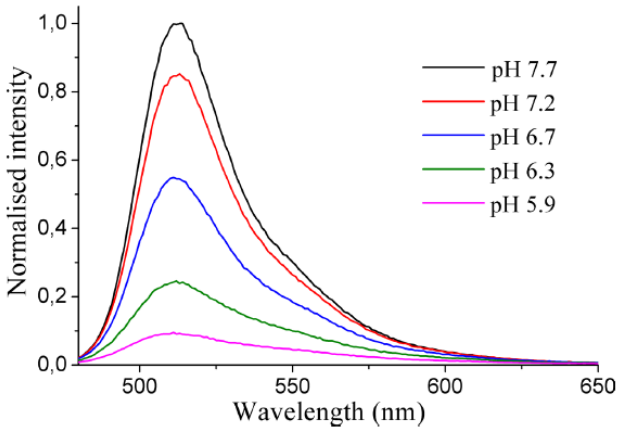

Figure 1.8: Fluorescence emission spectrum of fluorescein depicted for different pH levels. Reprinted from [43]

1.5.2. HPTS

Another widely used fluorescent indicator dye is 8-Hydroxypyrene-1,3,6-trisulfonic acid (HPTS). This is due to the fact that HPTS is water soluble, non-toxix and highly photostable [34]. Furthermore, it has a pKa of 7.3 [44] which is in the physiological range. Moreover, it has a bright yellow fluorescence emission which has a 600 fold increase in intensity over the pH range of 4-8 [45]. In Figure 1.9, the molecular structure of HPTS is shown. In the figure both the protonated and the deprotonated form of HPTS are shown. These two forms of HPTS both have their own excitation peak wavelength, which is ̃405nm for the protonated form and 460nm for the deprotonated form and both emit at 510nm. When using recordings of emission at 510nm for both excitation wavelengths and taking the ratio of them as is shown in Equation 1.13, ratiometric sensing is made possible. As described in 1.4.1, the use of ratiometric sensing decreases the influence of indicator concentration, illumination intensity and detector sensitivity. HPTS is widely used in biosensing applications due to its biocompatibility. However, due to the high water solubility of HTPS, it needs to be physically entrapped or covalently bonded to a support matrix in order to prevent dye leaching. Which would decrease the performance of the sensor significantly. Different types of support matrices will be discussed in Section 1.6. Another disadvantage of HPTS is the sensitivity to ionic strength. This is due to the amount of nagatively loaded function groups of the molecule which is 3 in the acidic form and 4 in the basic form [23]. This leads to a shift in pKa values which can be of the magnitude of 0.5pH units. Therefore, special care must be taken to correct for this influence on the pH measurements when the ionic strength of the sensor environment differs significantly.

$$R = \frac{I_{510}(\text{excited at 460nm})}{I_{510}(\text{excited at 405nm})} \tag{1.13}$$

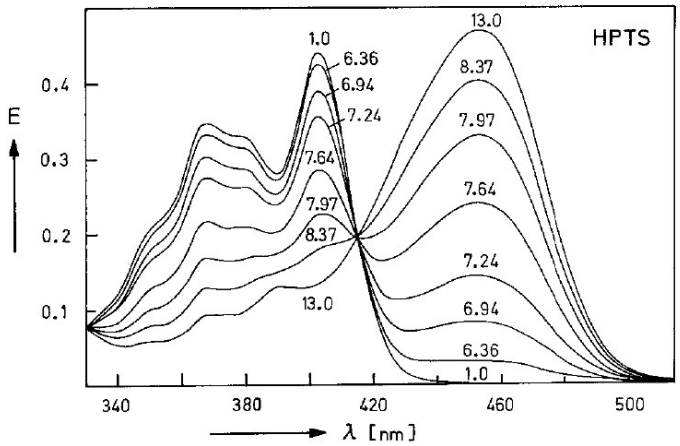

Figure 1.10: Excitation spectrum of HPTS measured at 510nm. As can be seen in the Figure the excitation peaks lay around 400nm and 460nm [47]

1.5.3. Benzoxanthene Dyes

The next group of indicator dyes that need to be discussed are the Benzoxanthene dyes. Among these dyes are the seminaphthofluoresceins (SNAFLs) and the seminaphthorhodafluors (SNARFs) which are recognizable by their benzene and naphthalene component [48]. These indicators typically have a pKa of around 7.5, which is close to the physiological range [49]. Moreover, they show distinctive emission from protonated and deprotonated molecules which enables ratiometric sensing. In SNARF, the fluorescence is stronger in the basic form, while in SNAFL, the acidic form is more fluorescent. A wide range of derivatives of these fluorophores are discussed in [49], with each a slightly different emission and excitation spectrum.

Another property of these dyes is that the absorption peaks shift as a function of pH. This can be seen in Figure 1.11 from [49], where absorption and emission spectra of the Benzoxanthene derivative C-SNARF-1 is shown. In the left image the absorption spectra can be seen for various pH level. It can be observed that the absorption peak is red shifted with increasing pH. In the right image the two emission peaks of the fluorophore can be seen which enables ratiometric sensing. Another example for this phenomenon is shown in [50], where C-SNAFL-1 was used as indicator dye for pH measurements in tumorous tissues of mice. It was observed that the indicator dye had two emission peaks one which was non sensitive for pH and stayed at 545nm but the other peak shifted from 587nm to 605nm when the pH was decreased from 7.25 to 6.3. The main disadvantage of the use of SNAFL is the low quantum yield which lays in the best cases around 0.5 [49]. Moreover, due to the shift in spectra as function of pH the efficiency of the fluorescence can be even lower. Another disadvantage is that the Benzoxanthene dyes are relatively expensive when compared with HPTS for example.

1.6. Support matrix

In the previous sections the properties of fluorescent materials are described. However, in practise these materials can seldom operate by themselves. Therefore, in most non invasive sensor applications the fluorescent material is used in combination with a support matrix. A support matrix is a material in which the fluorescent material is immobilized. The immobilization of the fluorescent dye is needed in most cases to offer stability, flexibility and permeability [51]. This is needed to prevent dye leaching and thus maintain the fluorescent capabilities of the material over a longer period of time. At the same time the matrix should be porous enough to facilitate the interaction between the analyte, in this case the H^+ particles, and the indicator dye [52]. Furthermore, it should be noted that after immobilization the indicator dye can alter some of its characteristics which can have a significant effect on the performance of the overall sensor.

The immobilization of indicator dyes can happen using multiple methods. These include adsorption, electrostatic binding, physical entrapment and covalent binding [53]. However, of these methods only

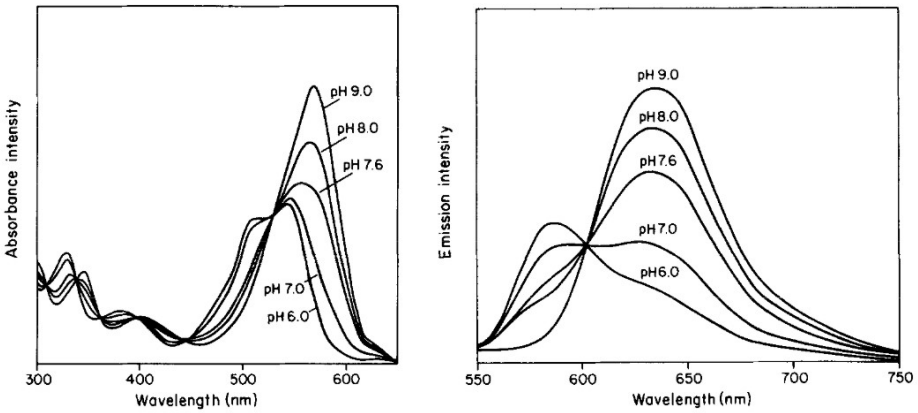

Figure 1.11: Absorption and emission spectrum of C-SNARF-1. It can be observed that the absorption peaks shown in the left figure are significantly red shifted with increasing pH. Furthermore, in the right figure two emission peaks can be seen, which enables ratiometric sensing. Reprinted from [49]

physical entrapment and covalent binding result in a stable and reproducible sensor material. Specifically covalent immobilization is preferred since this prevents the indicator dye from leaching from the supporting material [54]. An overview of the advantages and disadvantages of these immobilization techniques are shown in Figure 1.12 from [55].

The most widely used support matrices can be divided into two groups the organic and inorganic polymers. In the following part the characteristics of these two groups will be discussed alongside their advantages and disadvantages.

Organic polymers Organic polymers are the most used kind of support matrices for fluorescence pH sensing applications [32]. Most of these polymers have a high affinity with water and are commonly called hydrogels. Hydrogels are a network of hydrophilic polymeric networks which have as main characteristic their water absorbing capabilities, hence their name hydrogel [56]. Aside from their water holding capabilities, hydrogels are also know for their permeability and biocompatibility [57]. Furthermore, due to their high water content hydrogels have a high flexibility making them well suitable for use as support matrix for a sensor layer [58]. However, the ability to absorb large amount of water also results in varying volume and geometrical orientation of the gel [59]. Therefore, when used for sensor applications this should be taken into account . Several different hydrogels are used as support matrix for fluorescence pH sensors such as the polyurethane based hydrogel D4 in [60], a natural occurring anionic polymer called alginate in [61] and PEG-diacrylate in [62].

Inorganic Sol-gels are a type of inorganic support matrices that are commonly used for fluorescent sensors. The sol-gel process typically entails the hydrolysis of a silicon alkoxide in solution (the sol). Whereafter, a network is formed by condensation polymerization at room temperature (the gel) [63]. Thereafter, an aging process takes place to remove the extra fluids in the gel and thus to densify the sensor layer [53]. At the sol stage the analyte sensitive dyes can be added, whereafter they will be completely entrapped which prevents dye leaching. Another, advantage of using sol-gels is their unique tailorability [64]. This is due to the fact that by varying the precursor types and aging procedure, the properties of the material can be altered significantly. However, this can also be counted as a disadvantage since this also complicates the production of a sensor layer which will fulfill very specific requirements. Examples of sol-gels that are used for fluorescence ph sensing include: Wencel et al. [64], where a combination of GPTMS and ETEOS was used as the precursors of the sol gel matrix which entrapped the indicator dye HPTS. This sensor was able to operate in the pH range from 5 to 8 with a response time of 12s. Another example by Grant et al. [65] made use of a combination of TMOS and PBS as the precursors of the support matrix. Thereafter, the indicator dye SNARF-1C was added. This resulted in a sensor which was able to sense in the pH range from 6.8 to 8 with a response time of less than 15s. The main disadvantage of this sensor is the fabrication which was reported to be more than a month.

Immobilization method	Advantages	Disadvantages
Adsorption (physical, ionic binding, chelation)	Simple Mild binding conditions Low biomolecule changes	Weak binding force Binding stability highly dependent on pH, solvent and temperature
Entrapment (gel entrapment, microencapsulation)	Mild procedure Intermediate binding forces Possible protection from microbiological attack High stability	Possible loss of biomolecule activity by leakage Denaturalization by free radicals formed in the process
Cross-linking	High stability Strong binding force Used for stabilization of proteins covalently bound to a solid support Possible protection from microbiological attack	Reaction difficult to control High amounts of biomolecule are required Possible loss of protein activity
Covalent binding	Stable binding Low leakage High stability	Time consuming and laborious reactions Activity losses if the groups required for the biological activity are involved in the binding

Figure 1.12: Main immobilization methods and their advantages and disadvantages. Reprinted from [55]

1.7. Optical system

In the previous sections the properties and choices of the sensor layer are described in detail. The function of the sensor layer is to change its fluorescence properties as function of the pH value of its environment. However, in order to measure this change in fluorescence an optical system is needed. This optical system will be discussed in this chapter. In the first section the general overview of a typical optical system for fluorescence sensing will be discussed. Thereafter, in the next sections the components of this system will be discussed and the different design choices will be compared. Lastly, the signal processing and the data analysis will be explained.

1.7.1. General overview

In Figure 1.13, a simple schematic of a optic system for detecting fluorescence can be seen. As can be seen from the figure the system begins with a light source. This source ideally transmits light in the range of the optimum excitation wavelength of the sensor layer. This light can be tuned in a more accurate way when a filter is placed between the light source and the sensor layer. However, this would make the whole system larger and more complicated. Therefore, this will only be used when it is absolutely necessary. Thereafter, the light will be absorbed by the sensor layer after which the layer emits fluorescent light which will be captured by a detector device whereafter the received signal will be processed by a computer to extract the measured pH value. In the next section these components will be discussed in more detail.

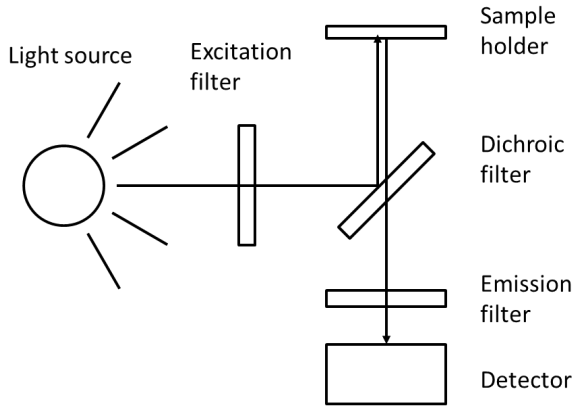

Figure 1.13: Typical fluorescence sensing setup. Reprinted from [66]

1.7.2. Optical components

The components of the optical system play a crucial role to obtain accurate and reliable measurement results. In this section the required properties and characteristics of the individual components will be discussed. Furthermore, different component options will be compared.

Light sources

Choosing the correct light source for your fluorescent sensing application is essential for its operation. A wide variety of light source are available to chose from and each of them has its own advantages and disadvantages. The important parameters of light sources include: emission wavelength, intensity, stability, power consumption and cost.

One of the most conventionally used light sources are arc or halogen lamps. These light sources typically emit a broad range of wavelengths from near infrared to ultraviolet. This means that these lamps can be used for the excitation of multiple fluorophores which have different excitation wavelengths. However, the broad wavelength spectrum of arc and halogen lamps is normally not uniform, which means that for the use of multiple fluorophores compensation will be needed to account for the intensity difference [67]. Furthermore, arc and halogen lamps have a relatively high power consumption. This means that these light sources will generate a substantial amount of heat which can be detrimental in medical applications. Another disadvantages of these lamps are that they are relatively large and are used mostly in a laboratory setup, which make them not suitable for the desired application.

Lasers (Light Amplification by Stimulated Emission of Radiation) are also widely used as light sources for fluorescence sensing applications. This is mostly due to their monochromatic characteristics, which means that lasers have a exceptionally narrow emission spectrum. This renders them highly suitable for fluorescence sensing applications. When the narrow emission spectrum of a laser aligns with the excitation spectrum of a fluorophore, the efficiency can be maximized. Another characteristic of lasers is their narrow light beam which makes it possible to focus the full intensity of the light beam on a small target surface area. Despite these advantages lasers are not suitable for the application described in this thesis. This is due to the fact that lasers are costly and require a relatively large and complicated system [68].

The last light source that will be discussed in this section are Light emitting diodes (LED). LED's are semiconductor devices which emit photons when a current is sent trough them. The wavelength and energy of this emitted light is related with the bandgap energy which is a material property of the semiconductor material [69]. Therefore, LEDs can emit light of a very specific wavelength. Therefore, when making use of several fluorophores with different excitation wavelengths, multiple LEDs will be needed. Other advantages of LEDs are their high power efficiency, long lifespan and offer good stability over time [70]. Furthermore, they can be very small and are inexpensive.

Detectors

Another key component of the optical system is the photodetector, which is responsible to capture the light emission of the fluorescent material and to convert it to an electronic signal, which can thereafter be processed. A good photodetector has a linear response to the intensity of the incident light over at

least several orders of magnitude [71]. In the past the most commonly used photodetectors for fluorescence applicationns were photomultiplier tubes (PMT). These devices consisted of a photocathode on which incident photons will trigger a flow of electrons. After a few cascading stages this flow of electrons can be measured. The advantage of these devices is that it can detect very low light levels as well as relatively high light levels. Furthermore, these device can measure with a very high accuracy. However, PMTs are relatively expensive, large and operate on a very high operating voltage of 2400 - 3000V. Therefore, these devices were commonly used in laboratory setups but are not suitable for compact applications such as described in this thesis.

A smaller and less costly alternative for the PMTs are the photodiodes. These are semiconductor devices which converts light into electric current. When the photons hit the photodiode electron hole pairs are generated. This process is called the photoeletric effect. The generated electron hole pairs are separated by the applied electric field. This movement of charge carriers generates a current which is proportional to the intensity of the incident light. The advantage of these devices is that they are cheap and small. However, it does not have intrinsic amplifier functions so for most sensor applications an external amplifier is needed. Furthermore, it can not accurately differentiate wavelengths so when a certain wavelength needs to be measure a filter will be necessary.

Other detectors that can be used are charge coupled devices (CCD) and complementary metal oxide semiconductor (CMOS) cameras. These are generally used when a two dimensional image is needed. CCD cameras are based on an array of capacitors which are able to store electric charge generated by incident light. After some time, also known as the integration time, the charge stored in the individual capacitors (pixels) will be transferred out of the CCD device and converted to a digital value. This is done sequentially for the individual pixels. Due to the sequential readout of the pixels the time it takes to capture a whole image is relatively long [72].

CMOS are comparable to the CCD devices. However, they do not consists of an array of capacitors but an array of pixels. These pixels consists of an photodiode, a capacitor and up to three transistors [73]. In this configuration the capacitor will be charged or discharged by the photodiode at an rate which is directly proportional to the incident light on the photodiode. After the integration time, the charge of the capacitor will be readout and converted into a digital value. The main difference between the CCD and the CMOS device is the fact that CMOS devices are able to perform the readout at the pixel itself and does not need sequential charge transfer as in the CCD. this means however, that in each pixel additional components are present which are not sensitive to incident light, which reduces the fill factor of the device. This problem can be solved partly by using lenses to direct the light onto the photodiode. The main advantages of these devices are their capability to supply high resolution 2 dimensional images. However, these do need more sophisticated software and signal processing to convert to an pH value than for instance compared with single photodiodes. Furthermore, the costs of these devices is significantly larger.

The last device that will be highlighted in this section are optical spectrometers. These devices are widely used in fluorescence microscopy. Spectrometers usually include one or more diffraction gratings, an optical path, and a detector array. Light enters through an input slit and is then directed onto a diffraction grating, which separates the light into its spectral components. A concave mirror then focuses this dispersed light onto the detector array [74]. A simplified schematic of spectrometer can be seen in Figure 1.14. The main advantage of these devices are their ability to precisely differentiate between wavelengths. However, they are relatively expensive when compared to photodiodes or CMOS cameras.

Filters

Depending on the fluorescence application and system configuration optical filters will be needed. The most commonly used filters in fluorescence applications are the excitation and emission filters and dichroic beamsplitters [76].

Excitation filters are used to selectively transmit light at the desired excitation wavelength. This is particularly needed when the excitation light source has a wide bandwidth and thus the filter can be used to make sure only the light at the excitation wavelength will be transmitted to the sample. This

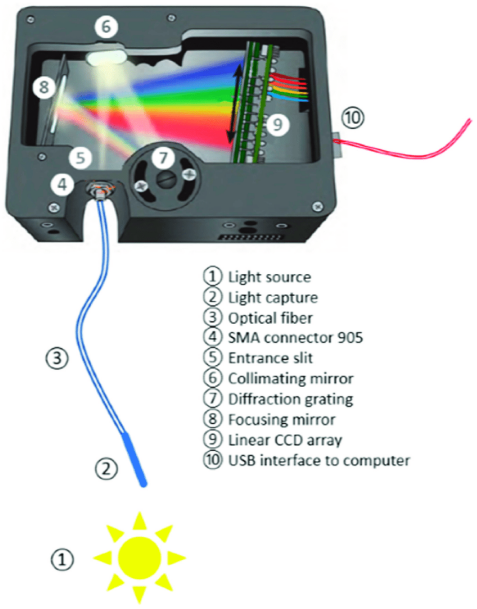

Figure 1.14: Inner workings of a typical optical spectrometer. Reprinted from [75]

will lead to less background noise and thus a larger signal to noise ratio. Excitation filters are typically bandpass filters narrow pass band around the optimal excitation wavelength.

Emission filters used to specifically transmit the fluorescent light emitted by the sample while blocking all other light. This ensures that only the light which contains the information of the sample is passed to the detector which increases sensitivity of the sensor. These filters are typically bandpass or longpass filters. However, as discussed in the previous section 1.7.2, this type of sensor is only needed when a camera or photodiode is used since a spectrometer is already able to distinguish between different wavelength and the intensity at specific wavelengths can easily be extracted.

Dichroic beamsplitters are another possible filter that can be used in a fluorescence sensing setup. A dichroic beamsplitter is usually positioned at a 45°angle with the light paths. Their function is to reflect the shorter wavelength excitation light from the light source to the sample and to transmit the longer wavelength emission light from the sample to the detector [77]. This kind of configuration is commonly used in fluorescence microscopes. In Figure 1.13, a typical schematic of such a configuration can be seen. In Figure 1.15, typical transmission characteristics of both the emission and excitation filters alongside the transmission characteristic of the dichroic beamsplitter is shown.

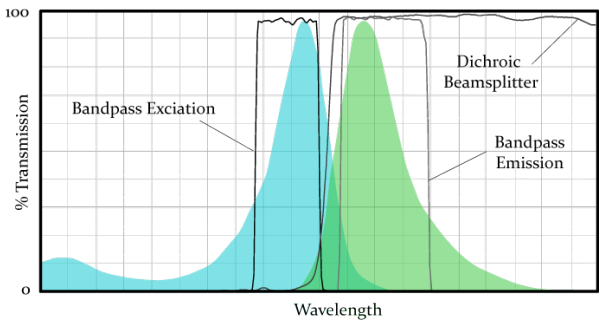

Figure 1.15: Typical transmission characteristics of the excitation and emission filters and the diochroic beamsplitter. Reprinted from [78]

2

Design choices

In the previous chapter, the basic principles of fluorescence sensing for pH measurements are discussed. In this chapter the design choices made for the design of the new pH sensor will be explained. In the first section several state of the art sensor will be highlighted. Thereafter, a choice of indicator dye in combination with support matrix will made.

2.1. State of the art

Before the design process of the new pH sensor first state of the art sensors need to be examined. This is to pick up on existing knowledge on which can be built on. Furthermore, the current limitations and pitfalls can be identified. In this section five state of the art sensors which are published in papers will be discussed.

The first sensor that will be discussed is the sensor designed by Li et al. [79]. This sensor was designed to track tumor micro environments. As indicator dye an HPTS derivative HPTS-IP is used. This dye is thereafter entrapped in a sol-gel consisting of 3-glycidoxypropyltrimethoxysilane (GPTMS) and Ethyltriethoxysilane (ETEOS), together with an anti-bleaching agent 1,4-diazabicyclo [2.2.2] octane (DABCO). Thereafter, a tapered optical fiber was dipped in this sol-gel mixture after which it was cured in an oven. The sensor thereafter, reported a resolution of 0.0050 ph units over a pH range of 5.5–7.4 and a response time of 4s. Furthermore, the sensor showed great reproducibility and biocompatibility. The main disadvantage of this sensor is the long and complicated fabrication as the total production time took 10 days. Furthermore, sophisticated laser equipment is used for excitation of the sensor layer.

The next sensor that will be discussed is the sensor designed by Bian et al. [80]. In this work a sensor was fabricated with the use of the fluorescent indicator dye 5(6)-carboxyfluorescein (5(6)-FAM), which is a fluorescein derivative, see section 1.5.1. This indicator dye was encapsulated in a hydrogel which was thereafter coated on an optical fiber. The sensor reported a resolution of 0.07 pH units in the range of 6-8 pH. Furthermore, the sensor was tested on pork tissue which proofs biocompatibility and feasibility for tissue measurements. The main disadvantage of this sensor is the low response time which was reported to be around 13 min.

Another fluorescent pH sensor was developed by Gong et al. [81]. The indicator dye used is the same as in the sensor described above by Bian et al. [80], 5(6)-FAM. However, in this sensor the 5(6)-FAM was combined with the reference dye PdTFPPT. The combination of these dyes made ratiometric measurements possible. These dyes are thereafter entrapped in polymer PA101. The sensor layer was fabricated with the use of an inkjet printer which deposited the polymer mix on glass slides. The sensor reported a good photo stability and robustness.Furthermore, the response time was around 16s. The same process was used in a later work of Gong [82], where a precision of 0.1 pH units was reported over a rang of 5.5 - 8 pH. The main advantage of these sensor is the complexity in the fabrication and the expensive and sophisticated machinery needed for this fabrication.

The last sensor that will be discussed is the sensor devised by Huo et al. [83]. This is combination of a colorimetric and fluorescent pH sensor. It uses the carbon quantum dots as indicator material which were used in combination with the support matrix Poly(m-phenylene isophthalamide) (PMIA). This sensor is based on the colorimetric changes of the fluorescence emission of the qunatum dots. These changes wawer measured by taking images with a smartphone and then processed using photoshop to get the RGB values of the captured images. This resulted in an accuracy of 0.2pH units and a response time of around 5s. The main disadvantage in this work is the complexity in the fabrication of the carbon dots and PMIA layer.

2.2. Fluorescent indicator dyes plus support matrix

In this section the result of the literary search for indicator dyes in combination with their support matrix will be discussed. In order to find the most suitable indicator dye, first the required specifications must be determined. This was done by Maurits Vriesendorp in his thesis in collaboration with a medical specialist [84]. A summary of the minimal specifications are listed in Table 2.1

Table 2.1: pH sensor requirements

pH range	6-7.5
Response time	30s
Accuracy	0.01
Size	3x3 cm
Drift	0.01 per hour

Along with these requirements the indicator dye should also be relatively simple to fabricate in order to make it feasible for the time period of the thesis. With these requirements in mind the literary search was performed.

The results of the search can be found in Table 2.2. As can be seen in the Table the advantages and disadvantages of the sensors mentioned in the papers are listed.

As can be seen from the Table, the sol-gel sensors have a better response time but are generally more complex to fabricate and require more time. The method used by Kermis [62] and Cattini [85], was already used in the thesis of Maurits Vriesendorop [84], this was due to the fact that it has a relatively simple fabrication process and good pH characteristics. Therefore it was chosen to continue the work described in [84]. In this work HPTS was used as a fluorescenct pH indicator dye in combination with the hydrogel Hydromed D4. However, due the high water solubility of HPTS and the large pore size of the hydrogel, HPTS would quickly leach out if not sufficiently immobilized. Therefore, anion exchange resin microbeads are used to immobilize the HPTS. Thereafter, the microbeads loaded with HPTS can be easily entrapped in the hydrogel support matrix.

2.3. Optical system

In this section the design choices regarding the optical system will be discussed. In order to make the correct choice first the requirements of the system should be considered.
As described in the previous section HPTS is chosen as indicator dye. This dye has two excitation peaks one at 405nm and one at 465nm. Therefore, the light sources uses in the optical system should be able to emit at these wavelengths or optical filters are needed. Furthermore, the detector of the system should be able to detect the emission peak wavelength of HPTS which is at 510nm. Alongside these requirements the system should be simple, small and inexpensive.

Taking these requirements into consideration. LEDs are chosen as light source for this sensor system. This due to the fact that they are small, inexpensive and are able to emit at very specific wavelengths. This also means that no excitation filter is needed which decreases the cost and size of the sensor system. As detector an optical fibre connected to a spectrometer is chosen. This combination makes it possible to have a sufficiently small detector area and to record a wide range of wavelengths. Moreover, the spectrometer can be connected to a computer which is able to select specific wavelength which ensures that no emission filters are needed decreasing the size of the system even more. In the next section the fabrication of the eventual sensor and sensor system will be discussed alongside the testing methodology.

Table 2.2

Author	Indicator dye	Support matrix	pH range	Response time	Advantages	Disadvantages
Kefeng Huo et al.	Carbon Quantum dots	PMIA	5-9	5s	• High accuracy • Broad pH range • Fast response	• Complicated fabrication process • Combination colorimetric en fluorescence sensor, so more complex read-out system needed.
Saying Dong et al.	cresol red, bromophenol blue and chlorophenol red	TEOS and TRITON	4.5-13	5s	• Good repeatability • Broad pH range • Fast response	• Relatively complicated process • Design of sensor is for liquid applications
Jingjing Gong et al.	(5(6)-FAM and Porphyrin	TMSPMA	5.5-8	30s	• Wide enough pH range • Fast response • Biocompatibility is proven	• Inkjet printer is needed • Polymerisation process is not precisely mentioned
Dorota Wencel et al.	HPTS	GPTMS-ETEOS solgel	6-8	2min	• Wide enough pH range • Biocompatibility is proven • relatively simple process	• Not very fast • sensitive to Ionic strength variations
Dorota Wencel et al.	HPTS-IP	GPTMS-ETEOS solgel	6-8	12s	• Fast response time • Simple fabrication process	• Experiments are performed in a flow cell so different application • Sensitive to Ionic strength variations
Qingsong Cui et al.	HPTS and CTAB	ETES:GLYMO	5.75-7.25	Not mentioned	• Simple fabrication process • Spin coating is used and parameters used are mentioned	• Response time not mentioned • HPTS used so probably also sensitvie to Ionic strength variations • Not vary broad pH range
Zesen Li et al.	HPTS-IP	GPTMS-ETEOS solgel	5.5–7.4	4s	• Fast response time • Great reproducibility • High resolution	• Long fabrication time;vv Sophisticated equipment needed
Zhenglan Bian	Carboxyfluorescein (5(6)-FAM) with PdTFPPT	polymer PA101	5.5–8	13min	• High accuracy • Great reproducibility • Tested with pork tissue	• Long response time
Haley Kermis et al.	HPTS	PEG hydrogel + microbeads	6–9	13min	• High accuracy • Easy fabrication	• Long response time
Stefano Cattini et al.	HPTS	Hydromed D4	4.11-9.50	not mentioned	• High accuracy • Easy fabrication • Chemicals already in house	• response time not menstioned

3

Method and Materials

During the project several experiments were conducted to come towards a functioning prototype sensor. In this section the methods and materials used to fabricate the sensors and conducting these experiments will be discussed.

3.1. Materials and Instruments

This section will discuss the materials, instruments, and equipment used for fabricating the sensor layers and conducting the measurements.

3.1.1. Materials

In this subsection the chemicals that have been used for the fabrication of the sensor layers and the pH buffers will be shown. Most of these chemicals have been reused from the thesis of Maurits Frans Vriesendorp [84]. 8- Hydroxypyrene-1,3,6-trisulfonic acid trisodium salt (HPTS product no. H1529), AmberChrom® 1X8 chloride form, strongly basic, 200x400 mesh (Dowex 1X8, product no. 44340), Ethanol (product no. 443611), Sodium phosphate dibasic dihydrate (NaH_2PO_4 product no. S0876-100G), Sodium Hydroxide solution 50% (NaOH product no. 415413- 25ml), Sodium Chloride 99.9% (NaCl, product no. S9888) and Hydrochloric acid 37% (HCl, product no. 320331) were all ordered from Sigma Aldrich (www.sigmaaldrich.com). Hydromed D4 (product no. 100028) was purchased from AdvanSource Biomaterials Corp (www.advbiomaterials.com).

3.1.2. Instruments and equipment

In order to fabricate the sensors and pH buffers, the following instruments were used: precise weight measurements of the chemicals were taken with a VWR microscale, and a magnetic stirrer from SI Analytics GmbH was used for mixing the chemicals. Additionally, two micro pipettes from VWR were employed for accurate volumetric measurements of fluids, one with a range of 50-200 µL and the other with a range of 200-1000 µL. Different glass slides have been used to deposit the HPTS hydrogel mixture upon. These include 75x21mmm glasses and 21x26mm glasses by Menzel-Gläser. Furthermore, for the production of the phosphate buffers the VOLTCRAFT PH-410 pH meter was used.

3.2. Methods

3.2.1. Fabricating the sensor layer

In this section the steps which were needed to create the first sensor will be explained in detail.

To start with, 35mg of HPTS is added to 100mL of deionized water and mixed together. Subsequently, 10g of Dowex microbeads is mixed with 10ml of deionized water. Thereafter, these two solutions are mixed together for 24 hours with a magnetic stirrer. After this time, a pipet is used to extract the excess water from the resulted solution so only the HPTS loaded microbeads are left.

In order to make sure the HPTS loaded microbeads would show the expected behaviour a small amount was divided over a basic and an acidic solution. According to the characteristics of HPTS the acidic solution should become transparant and the basic solution should become a yellow/green colour.

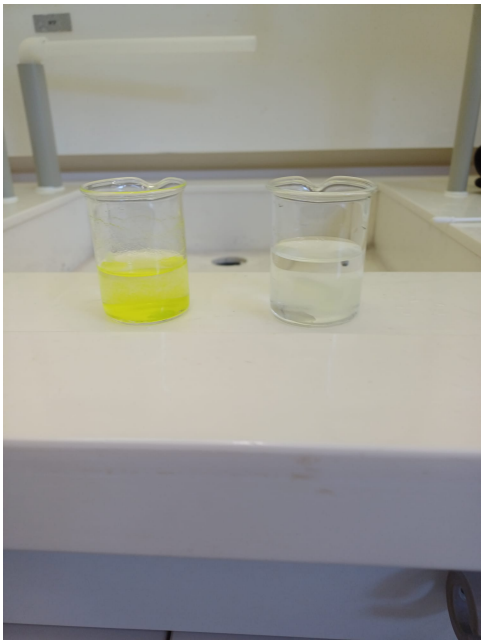

Figure 3.1: Microbeads added to basic and acidic solutions. Where the basic solution is shown on the left side and the acidic solution on the right side

As can be seen in Figure 3.1, the HPTS loaded microbeads function as expected.

In order to make the hydrogel, 1g of hydromed is suspended in a mixture of 9ml ethanol and 1ml deionized water. This is mixed with a magnetic stirrer for 6h until the hydromed is fully dissolved. Thereafter, 3.5g of the HPTS loaded microbeads are added to the hydrogel solution and mixed together for another 4 hours, see Figure 3.2a. After this time, 200 μL of this mixture is pipetted on thin glass slides, to create the actual sensor layer. This is then dried at room temperature for 12h. The result can be seen in Figure 3.2b.

(a) HPTS, microbeads and hydrogel mixed together

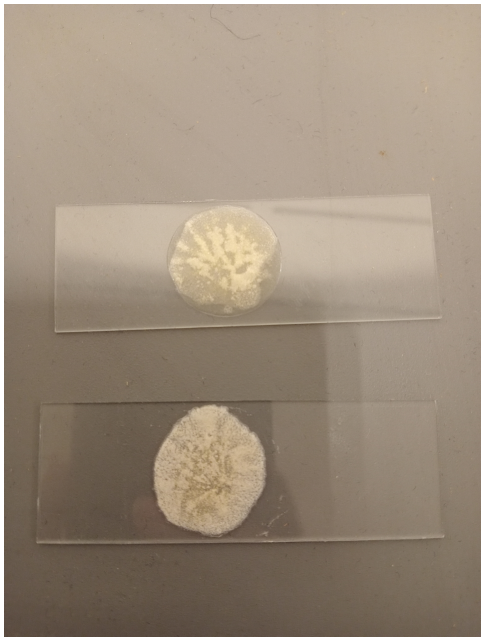

(b) The first fabricated sensor layers on thin glass slides

Figure 3.2: Last step and result of the production process of the sensor layers

3.2.2. Preliminary measurements

In the previous section the fabrication of the sensors is discussed. In this section the performed tests on these sensors will be explained.

The objective of the first tests was to see the relation between pH levels and measured intensity of the sample. This test was performed using a test setup which can be seen in Figure 3.4. As can be seen from the figure, the setup consists of a standard on which the sensor can be placed. Underneath the standard the LED is placed to illuminate the sensor layer from the bottom. Alongside the LED an optical fiber is placed which collects the excited fluorescent light and sends it to the spectrometer. By positioning the LED and the optical fiber underneath the sensor layer it makes it possible to pippet the pH buffer solutions on the layer from the top. A picture of the used led circuit can be seen in Figure 3.3. As can be seen in the figure, a light pipe is attached to the led in order to focus the light to a specific point.

The used LED was rated for a maximum intensity at 475nm which is the excitation peak for HPTS.

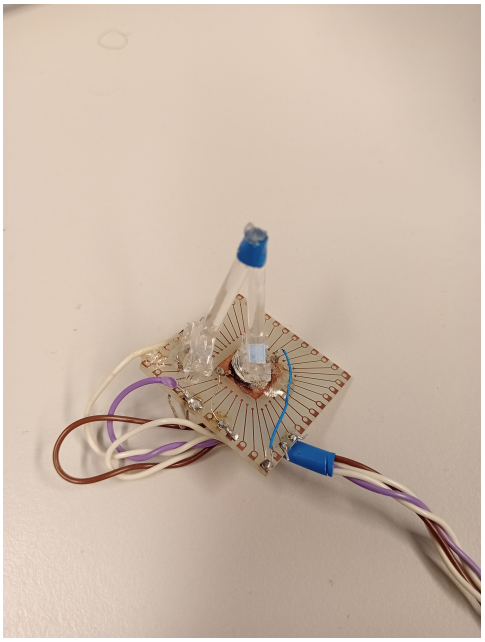

Figure 3.3: LED with light pipes used for the first measurements

In order to obtain the relation between the measured fluorescence intensity of the sensor layer and the pH level, pH buffers were used ranging from a pH level of 6.2 to 8.2 with increments of 0.4 pH units. These pH buffer solution were applied to the sensor layer using a micropipette which deposited $50\mu L$ of the solution on the sensor layer. Thereafter, 15 minutes was waited to be sure the sensor layer reached its equilibrium state, whereafter the sensor layer was rinsed with deionized water and patted dry with a paper towel. Thereafter, the next pH buffer solution was deposited on the sensor. This process was repeated for each pH buffer solution. This measurements showed the relation between the pH level and the intensity of the fluorescence. The measurements themselves were made by the flame spectrometer. This spectrometer was connected to a laptop with an USB cable. The spectra could than be seen in the program OceanView. This program was capable of saving the measured spectra as .txt files which thereafter, could be loaded into MATLAB, where the spectra could be plotted using the script shown in Appendix A.3. Another MATLAB script was used to extract the measured intensity at 525nm from the spectrum. This script can be found in Appendix A.1. This was done for all the measurements, whereafter the pH curve could be plotted which can be seen in chapter 4. Furthermore, from the obtained data points a calibration curve could be fitted. This was done by fitting a sigmoid function to the plotted data point, see Equation 3.1.

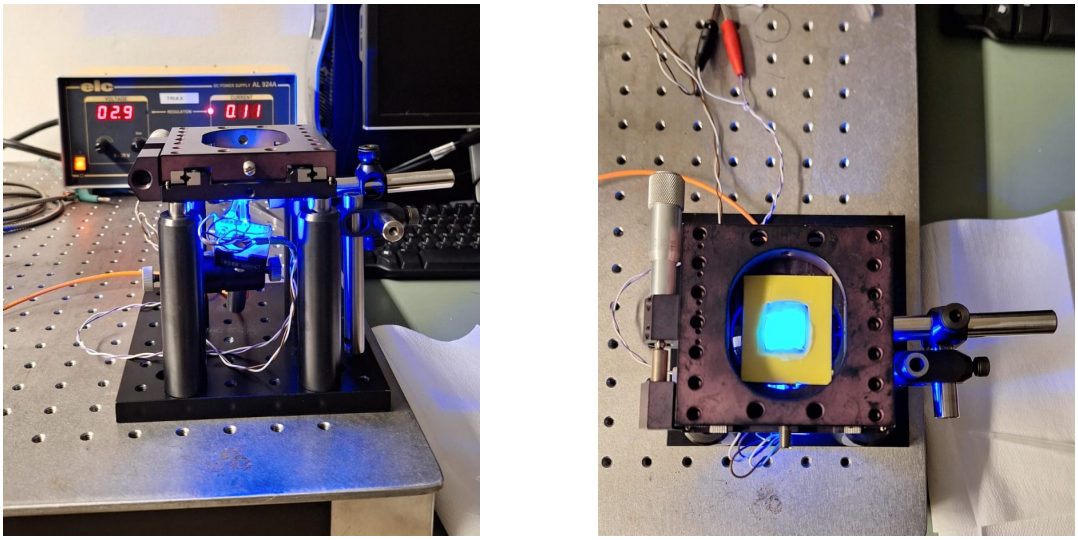

(a) Setup from the side

(b) Setup from the top

Figure 3.4: A figure with two subfigures

$$F = d + \frac{a - d}{1 + \frac{x}{c}^b} \tag{3.1}$$

Another important parameter that needed to be measured was the response time, since this needs to be sufficiently small to detect pH differences in a timely manner. This experiment was conducted by first applying the pH buffer of 6.2 pH. Then 20 min was waited to be sure that the sensor reached an equilibrium state. Then the measurements was started and each half second a measurement was recorded. Subsequently the pH buffer of 8.2 pH was deposited on the sensor. After 5 minutes of recording, the measurements were stopped since it became abundantly clear that the sensor reached an equilibrium again. The MATLAB code used for these measurements can be found in Appendix A.2.

3.2.3. Ratiometric measurements

The objective of the second measurements is to implement ratiometric sensing. As said in Section 1.4.1, fluorescence intensity is dependent on a lot of parameters. The influence of some of these parameters, including the geometrical alignment of the measurement setup and photobleaching, can be negated by using ratiometric sensing. In order to achieve ratiometric measurements for this application, two LED's are needed. One with a peak wavelength at 450nm and one with a peak wavelength of 405nm. This is due to the fact that it was stated that HPTS has two excitation peaks, see Section 1.5.2. These two LEDs are soldered on a prototype board after which light pipes were installed on the LEDs to ensure that both LEDs illuminate the same area. The built LED circuit ended up looking like the one shown in Figure 3.3.

Thereafter, the same measurements as discussed in the previous section were performed using the same spectrometer. The difference was that this time two recordings were made per pH value: one with 450nm LED on and one with the 405nm LED. Thereafter, the measurements are processed by using a MATLAB script. This script locates the peaks at the specified 525nm wavelength for both illumination wavelengths. The code of the script can be seen in the Appendix A.1

According to literature the fluorescence intensity of HPTS should be proportional to pH when illuminated with 450nm. Subsequently, the intensity should be inversely proportional to pH when illuminated with 405nm. For both these measurements the emission of 525nm is taken. By using both these measurements, the sensitivity of the whole sensor should be increased.

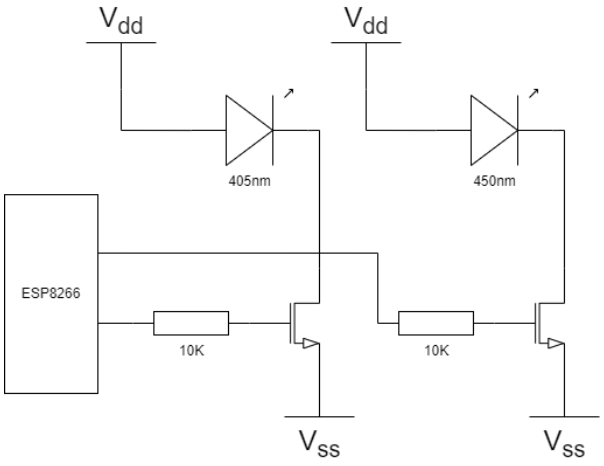

Figure 3.5: Schematic of the LED circuit. This circuit made it possible to control the LEDs using the ESP module which subsequently could be controlled using Matlab

3.3. Fabrication of whole sensor system

After the implementation of ratiometric sensing in the previous chapter, all the sensor components were in place to fabricate the whole sensor system. First the LED circuit was designed which can be seen in Figure 3.5. As can be seen from the figure two LEDs, one who emits 405 nm light and the other who emits 450 nm light, are connected to MOSFETs. Subsequently, the gates of the MOSFETs are connected to the ESP module. Therefore, the ESP module is able to open and close the MOSFETs and thus to turn the LEDs on or off.

The circuit described in Figure 3.5, was implemented on a prototype board of the ESP-module. This module was connected to a computer using an USB-cable. Furthermore, the ESP-module and the LEDs were connected to a power supply. As detector the flame spectrometer was used in combination with an optical fiber, just as in the previous measurements. In order to align the LEDs and the spectrometer in such a way that the sensor layer can be illuminated efficiently and the fluorescent light falls directly on the optical fiber, a case was designed. This case was designed in SolidEdge and thereafter, 3D printed. This case consists of two parts. On one part the LEDs are mounted. In this part also a hole is made to tightly fit the optical fiber. The other part of the case is the cover on which the glass slide with the sensor layer is glued. Thereafter, the cover part can slide over the first part with the LEDs which results in a closed off square box. In Figure 3.6, the a diagram of the whole system can be seen. On the right part of the figure a cross section of the sensor is shown. As you can see from the figure the sensor itself is connected to the esp module via power cables to turn the LEDs on and off. Furthermore, the sensor is connected via an optical fiber to the flame spectrometer in order to obtain the fluorescence measurement. Thereafter, the spectrometer sends the obtained data to the computer where it can be processed.

3.3.1. Total system testing

Now that the whole sensor system is produced it needs to be tested. The test setup can be seen in Figure. As said in the previous section both the ESP module and the spectrometer are connected to the computer. This makes it possible to control the whole system with MATLAB. Therefore, a MATLAB script has been written which is able to switch the LEDs on and off and trigger the spectrometer to obtain the spectra and save them. This script can be found in Appendix A.4. The first measurements that were performed, were comparable with the measurements discussed in the previous section. The main difference was that with this configuration the LEDs did not have to be manually connected and disconnected to the power supply, since that is now done by the ESP module.

Several batches of sensor layers are made to test different aspects and fabrication methods. The result are plotted using the MATLAB script shown in Appendix A.5.

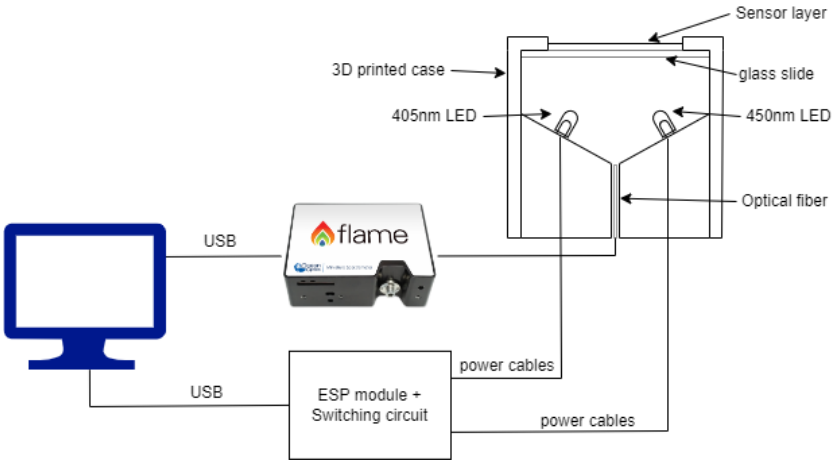

Figure 3.6: Schematic overview of sensor setup

Batch 1

The first batch of sensor layers are fabricated the with same procedure as discussed in section 3.2.1. The batch consisted of two sensors: one which was stored in a dry environment and the other was stored in deionized water. These two sensor layers were then tested using the same pH buffers as in the previous measurements. The spectrometer settings were set to an integration time of 1ms and 30 scans averaged for one measurement. The measurements started with the pH buffer of 6.2 which was deposited on the sensor layer. After 15min the measurement was taken after which the sensor was patted dry and the next buffer was deposited on the sensor layer. This was done for all the buffers up to a pH value of 8.2. The results are shown in Section 4.3.1.

Batch 2

The second batch of sensors was made to test the reproducibility of the results. In other words the sensors are tested to see if they give the same results in subsequent measurement. Therefore, the same methodology is used as in the previous section. So at the start of the measurement the pH buffer of 6.2 was deposited on the sensor. Thereafter, 15 minutes was waited after which the recording was made, whereafter the following pH buffer solution was applied. This was done for all buffers till 8.2. This measurement was performed three times with 20 min between the measurements. The results are shown in Section 4.3.2.

Batch 3

The third batch was fabricated with the objective to see how reproducible the sensor results were. This was done by fabricating 6 the same sensors following the protocol described in Section 3.2.1. These 6 sensor were fabricated to deposit a different pH buffer on each sensor. This differs from the procedure used previously, since now the influence of earlier applied pH buffers will be negated. A picture of these six sensors can be seen in Figure 3.7. This measurement was repeated for 4 times with the objective to investigate the reproducibility of the sensor layers. The result of these measurements are shown in Section 4.3.3.

Batch 4

For the fourth batch of sensor layers a small change has been made in the fabricating procedure. This is due to the fact of the variability in the results of the previous batches. This means that the stability of the sensor layers was poor. This could have many reasons. On of which was the fabrication procedure. During the fabrication of the previous batches the microbeads are mixed with the HPTS solution. This should result in HPTS loaded microbeads. Thereafter, the resulting solution is left for a certain amount of time to make sure the microbeads have sinked to the bottom of the glass. Whereafter, the fluid can be extracted leaving only the microbeads in the glass beaker. However, this does not guarantee that some of the HPTS that is not bonded with the microbeads is fully removed from the solution. Therefore, it could be that once the microbeads solution is added to the hydrogel mixture, some loose

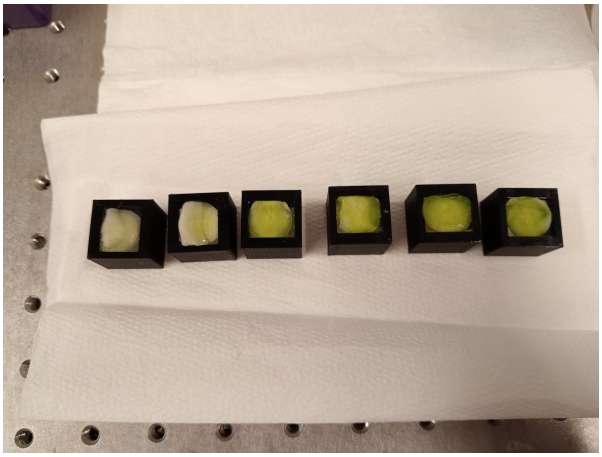

Figure 3.7: Six sensors used in the measurement where on each sensor a different pH buffer is deposited, ranging from the 6.2 pH buffer solution on the left to the 8.2 pH buffer solution on the right.

HPTS molecules can be transferred with it. This could then lead to a sensor layer with unbounded HPTS molecules which leach out over time and would thus result in a varying response.
In order to mitigate this effect, in this batch HPTS microbeads are rinsed two times to make sure that at least most of the HPTS molecules are removed so they cannnot have large influence on the response of the sensor layer. The measurements themselves are performed in the same way as in the previous batch. This time the measurement was performed 3 times for the same sensor to see if the reproducibility of the results have improved. The results are shown in Section 4.3.4.

Batch 5

For this batch of sensors new pH buffers were made. This had two reasons: One was to obtain more data points. Since in previous measurements only 6 pH buffers were used resulting thus in 6 data points. In order to get a better view of the behaviour of the sensors more data point are needed. The second reason was to make sure that the whole sensor layer could be submerged in the pH buffer. This is to make sure their can be no discrepancies between measurements due to non uniform buffer distribution on the sensor layer.

The pH buffers are produced using the fabricating procedure discussed in the thesis of Vriesendorp [84]. First a phospate buffer solution was made by dissolving 1.2g of Sodium Dihydrogen phosphate NaH_2PO_4 in 1 L of deionized water. Thereafter, an acid solution and a basic solution was made by using hydrogen chloride (HCL) and Sodium hydroxide (NaOH) respectively. For each pH buffer 90mL of the phosphate buffer was put in a glass beaker thereafter sodium chloride is added to obtain the same ionic strength as blood 150mmol. Thereafter, a pH meter is put in the beaker and by titration of the acid or base solutions the desired pH value is obtained. In Figure 3.8, the setup used for the fabrication of the pH buffers is shown. Using this method pH buffers ranging in pH value from 6.2 to 8.2 with increments of 0.2 pH unit were obtained, which resulted in 11 separate pH buffers.

After the fabrication of the pH buffers. The measurements were performed. This was done by putting a small portion of the pH buffer in a plastic container in which the sensor could be put in, with the sensor layer facing downwards. Thereafter, 10 minutes were waited after which the recording was made. This was then repeated for all the 11 pH buffers. This measurements was repeated for three times to see if the reproducibility was improved using this method. The results can be seen in Section 4.3.5

Batch 6

The last batch was fabricated to measure the response time again, but now for the whole sensor system. Furthermore, a new MATLAB script was written to do these measurement. This script can be found in Appendix A.6. This code takes a ratiometric measurement each second. The runtime was set to 400 cycles, ensuring the sensor would definitely be in equilibrium by then.

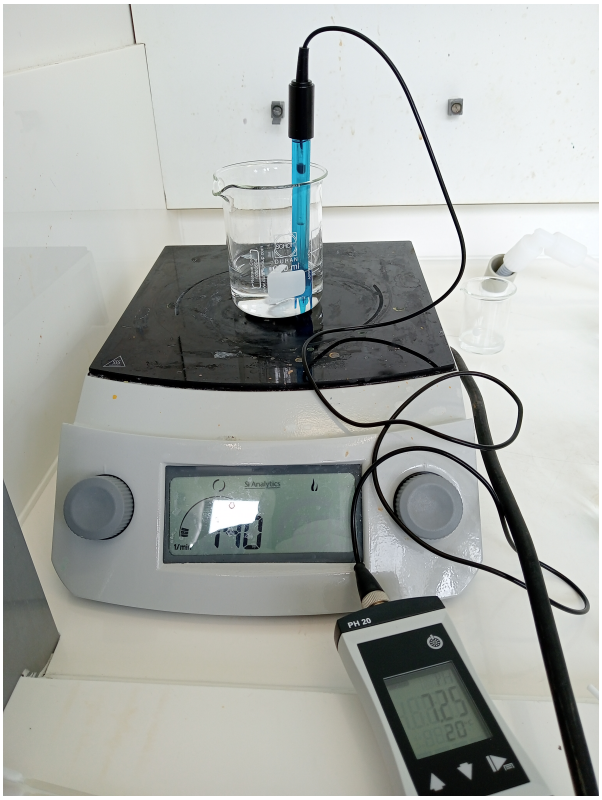

Figure 3.8: Fabrication of the buffer solutions using a magnetic mixer and pH meter

Two different measurements have been performed to see the response time of the sensor. The first measurement was performed by taking the following steps:

- The sensor was placed in a buffer solution with a pH of 6.2 for 15 min
- The measurement started
- After a couple of seconds, the sensor was transferred from the 6.2 pH buffer to a 8.2 pH buffer
- After 400 cycles the measurement stopped

The sensor was not immediately transferred from 6.2 to 8.2 to be sure that the initial sensor value could be measured.

Thereafter, the second measurement was performed which is followed the same steps shown above. However, in this case the pH sensor started in a pH buffer solution of 8.2 and was transferred to a buffer solution of 6.2. These measurement were then plotted using the MATLAB script shown in Appendix A.7 The results of these measurements can be seen in Section 4.3.6

4

Results

In this chapter the results of the measurements discussed in Chapter 3, will be shown and discussed.

4.1. Preliminary measurements

The spectra of the fluorescence emission due to excitation by the 475nm LED are shown in Figure 4.1a.

As discussed in earlier chapters the emission wavelength of interest is 520nm. From the picture it can be seen that the peaks of the spectra at this wavelength increase as function of pH which is as expected.

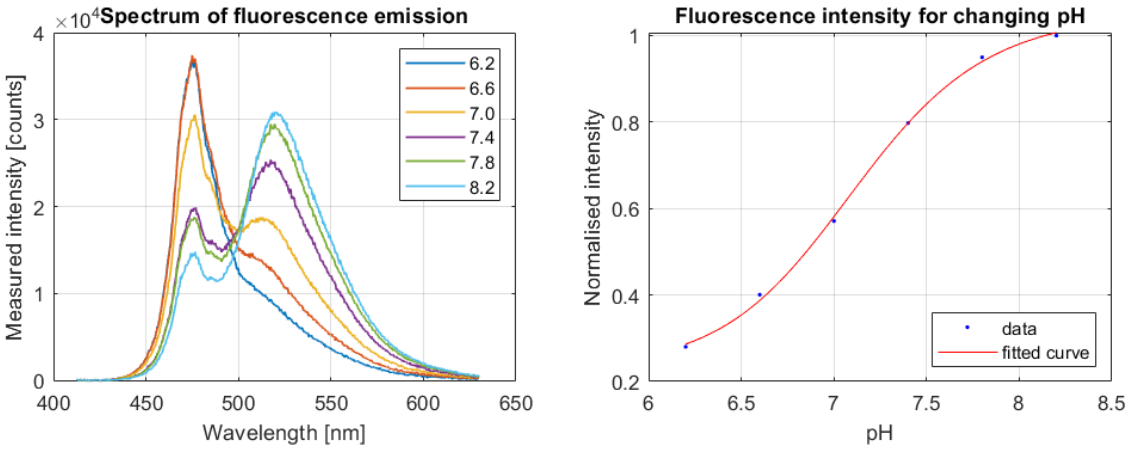

(a) Spectra of the first measurement for different pH values

(b) Normalised intensity of the fluorescence emission as a function of pH, with fitting curve

Figure 4.1: Result of the first measurement using only the LED with peak illumination at 475nm

In Figure 4.1b , the maximum of the spectra are plotted against the pH value, whereafter, fitting curve is used to estimate the relation between the data points. As can be seen from the figure the curve is well fitted with a root mean square error of 0.0150.

In Figure 4.2, the intensity of the fluorescence is plotted over time when the pH is increased from 6.2 to 8.2. The red dotted line indicates the time instance at which the pH buffer of 8.2 is applied to the sensor layer. As can be seen from the figure the response time is well below 20s. The difference between the normalised intensities of Figure 4.1b and Figure 4.2 can be attributed to the fact that during this first stage of measurements the measurements setup was not as unchanging as wanted. Therefore, slight changes in the position and orientation of the spectrometer occurred which led to differences in the measured intensities. This being preliminary measurements with the objective to find out if the material behaved satisfactory and as expected, these slight difference were not a problem.

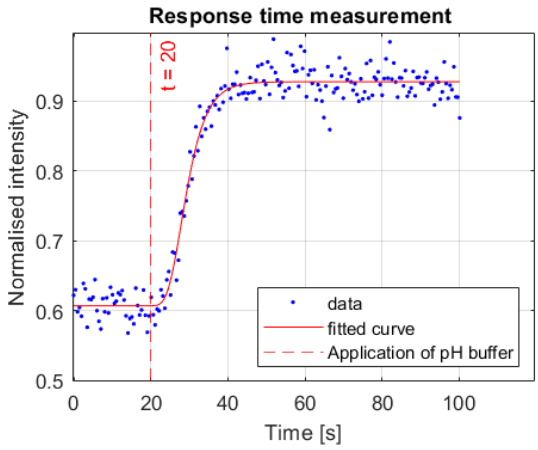

Figure 4.2: Response time measurements with the first designed sensor

Furthermore, in the figure a wide spread in measurement points can be seen. This is due to the fact that the measurements have been conducted without the use of the averaging function. This will be used in the future to get a more stable output response.

From both measurements discussed in this section it can be concluded that a clear relation between the pH and fluorescence emission is showing. Furthermore, response time of the fabricated is already within the required time which shows great promise for the final sensor.

4.2. Ratiometric measurement

As discussed in Section 3.2.3, the objective of these measurements were to see the effect of the implementation of ratiometric sensing. The spectra of the first measurements can be seen in figure 4.3. in Figure 4.4, both the intensities at 520nm are taken for different pH values. As discussed in Section 1.5.2, the intensity measured at this wavelength should increase with pH when illuminated with 475nm light and should decrease with pH when illuminated with 405nm light. However, as can be seen from both Figure 4.3 and Figure 4.4, for both illumination sources the fluorescence emission intensity increases with pH, which is thus contradictory to literature discussed in section 1.5.2.

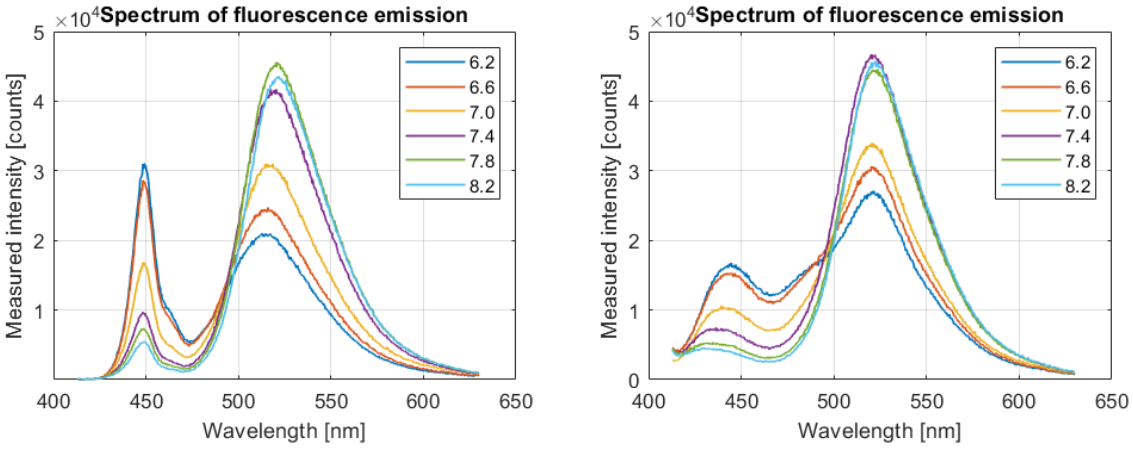

(a) 450nm illumination

(b) 405nm illumination

Figure 4.3: Spectra of fluorescence intensities at different pH values

In order to find the cause of this unexpected behaviour of the sensor layers, several small tests have been conducted. The first test was to see whether the microbeads and hydrogel would have an influence on the fluorescence behaviour of the sensor layer. This was done by making a sensing layer with only the microbeads and the hydrogel. This way it can be seen if by exciting it with the LEDs,

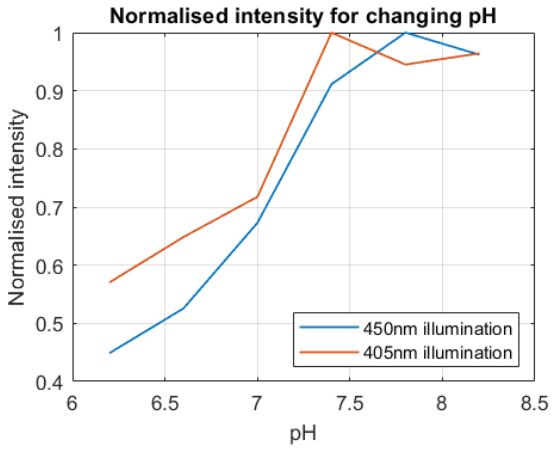

Figure 4.4: Normalised fluorescence intensity for different illumination wavelengths measured at 520nm

a pH dependency can be seen. If this is not the case, the microbeads and hydrogel do not have an influence on the fluorescence emission and are therefore, not the cause of the unexpected behaviour. The results of these test can be seen in Figure 4.5. As can be seen from the figure, there is clearly no relation between the pH value and the fluorescence emission. Therefore, it can be concluded that the microbeads and hydrogel are not the cause for the unexpected behaviour.

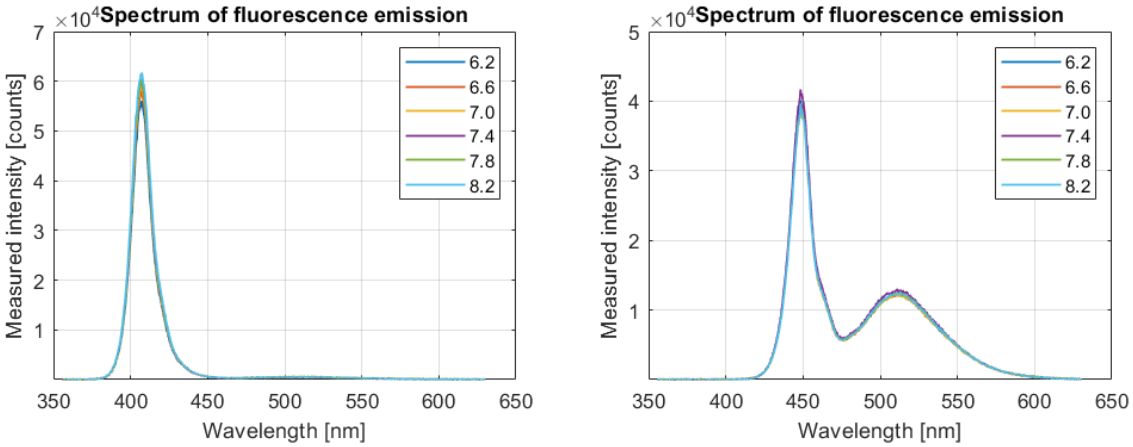

(a) 405nm illumination

(b) 450nm illumination

Figure 4.5: Spectra of fluorescence intensities at different pH values for sensor layer without HPTS

Another plausible cause is that the measurements are performed with relatively high powered LEDs using 100mA. Therefore, it was tested to see if the use of lower current would make difference for the pH sensitivity. This has been done by turning the power supply to 20mA. Thereafter, two measurements were made one when the pH buffer of 6.2 was deposited on the sensor layer and one where the pH buffer of 8.2 was used. The results can be seen in Figure 4.6. From the figure it can be seen that the fluorescence emission increases with pH for illumination by 405nm (figure 4.6b) and for illumination by 450nm (figure 4.6a). Which means that the current level did not have a significant influence on the sensitivity to pH.

These two tests did not give a satisfying explanation for the observed behaviour. This will be discussed in more depth in Chapter 5.

However, it can be seen from the spectrum shown in Figure 4.3b, that the UV emission is inversely proportional with the pH value when observed around the wavelength of 435nm which is not as expected, but can be used instead of the expected emission at 520nm.

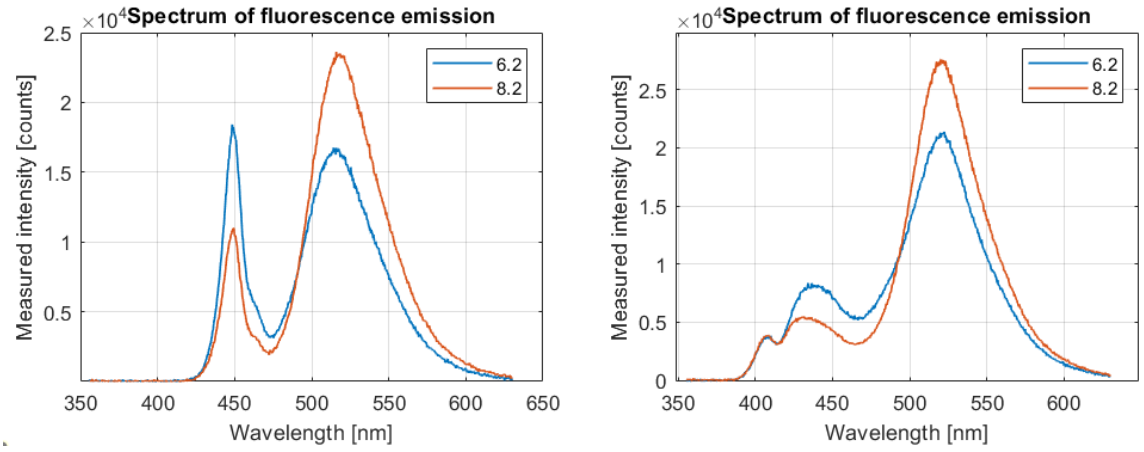

(a) 450nm illumination

(b) 405nm illumination

Figure 4.6: Spectra of fluorescence intensities when 20mA is used

By using the emission peaks obtained by measuring the 435nm and 520 fluorescence emission of the samples when illuminated with 405nm and 450nm respectively, the plots shown in Figure 4.7a are obtained. The blue one represents the fluorescence emission measured at 520nm when illuminated with 450nm light. The red line represents the fluorescence emission measured at 435nm when illuminated with 405nm light. When taking the ratio of these two plots ratiometric sensing can be implemented, by changing Equation 1.13, to Equation 4.1.

$$R = \frac{I_{510}(\text{excited at 450nm})}{I_{435}(\text{excited at 405nm})} \tag{4.1}$$

The result can be seen in Figure 4.7b. As can be seen from the figure the ratio of measured intensities shows a more than 8 fold increase over the pH range from 6.2 to 8.2.

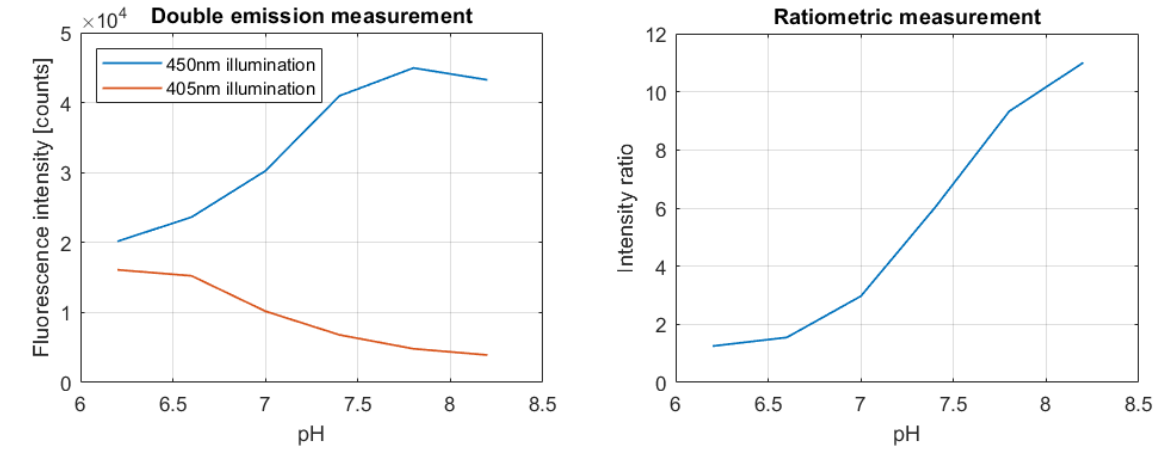

(a) Fluorescent emission measured at 520nm and 435nm when excited with 450nm and 405 respectively, for different pH values

(b) Ratio of the curves shown in Figure 4.7a

Figure 4.7: Implementation of dual excitation/dual emission ratiometric sensing

4.3. Total system

In this section the measurement results of the whole sensor system will be shown and discussed. As said in the previous chapter, the several batches of sensor layers have been produced to to test different aspects of the sensor and various fabrication methods.

4.3.1. First batch

In Figure 4.8, the first ratiometric measurement results can be seen for the fist two sensor layers which are measured using the whole sensor system. The sensors were stored for one day after fabrication. One of the sensors was stored dry and one of the sensor was stored in deionized water. As can be seen from the Figure the sensor which was stored in deionized water had a significantly better sensitivity.

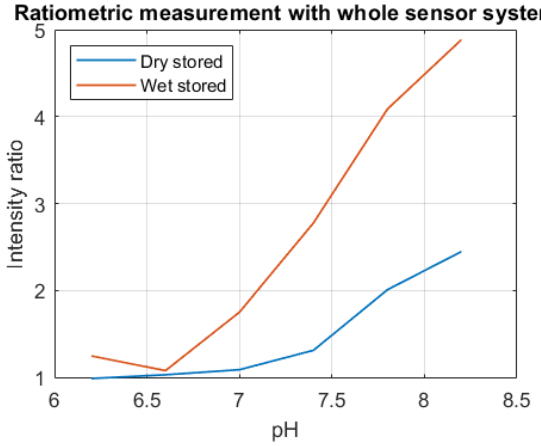

Figure 4.8: Ratiometric measurements with the use of the whole sensor system

4.3.2. Second batch

In this section the results of the first reproducibility tests are shown. As can be seen in Figure 4.9, the sensor shows no great reproducibility, since there is a large difference between the plots of the different measurement, both in magnitude as well as in sensitivity. One of the main reasons could be that for each measurement the buffer solution is distributed differently over the sensor layer, this mostly due to the fact that the hydrogel deforms when it comes in contact with water. However, in order to asses the true nature of these discrepancies, several other measurements will be necessary.

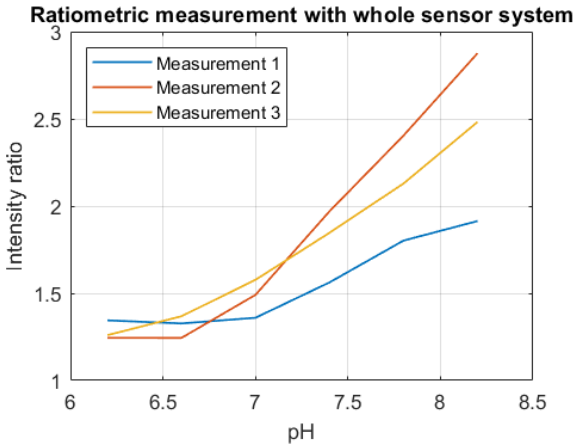

Figure 4.9: Ratiometric measurements with the use of the whole sensor system performed 3 times with the same sensor

4.3.3. Third batch

In Figure 4.10, the result of the measurements discussed in Section 3.3.1 are shown. The objective of these measurements was to determine with new measurement protocol the reproducibility and stability of the sensor layers. However, as can be seen in the figure the result does not show great reproducibility as there are significant differences between the measurements and also the trend is not as it should. For example when looking at the transition from pH 7.0 to pH 7.4 it can be seen that the curve goes downwards instead of upwards, which is opposite to what is seen in previous measurements. This

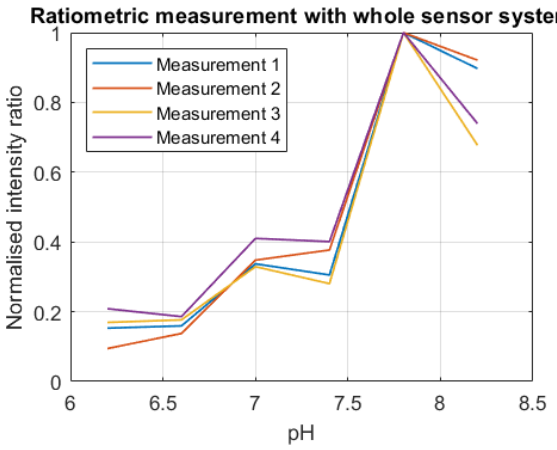

Figure 4.10: Ratiometric measurement where each point is a different sensor on which a different pH buffer is deposited. This measurement has been repeated 4 times

can mostly be attributed to the large difference in response between the different sensor layers, which makes them not comparable.

4.3.4. Fourth batch

As said in Section different sensor were fabricated with a slight change in the fabrication process. The results are shown in Figure 4.11, where three measurements of the same sensor are shown. As can be seen from the figure the result is not perfect but shows a large improvement over the reproducibility shown in earlier measurements. Especially in the pH range of 6.6-7.4, the slope of the curves are almost equal allowing for one point calibration. Although some measurement error can be seen in the curve of measurement 3, the yellow line. It can be seen that the measurement of the pH value 6.2 returned an unlikely high result. This can be attributed to the fact that the measurements are performed after previous measurement which ended with the pH buffer of 8.2. It could be that this buffer solution is not yet cleared completely out of the sensor layer which would result in a higher resulting measurements.

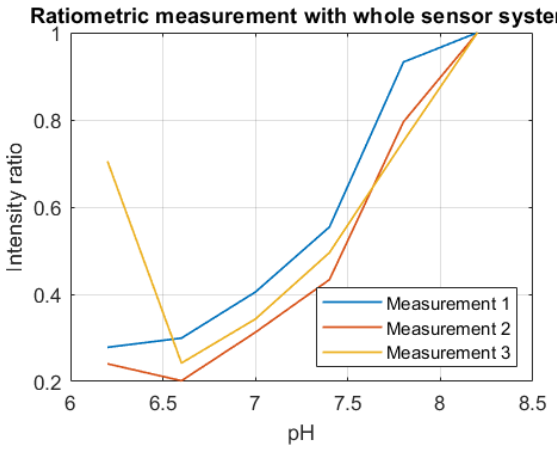

Figure 4.11: Three measurements with the same sensor after using the new fabrication method

4.3.5. Fifth batch

In Figure 4.12, the result of the measurements using the newly fabricated pH buffers is shown. As can be seen from the Figure the variance between the different measurements are considerably smaller than in previous measurements. Therefore, it can be concluded that the method of rinsing the mi-

crobeads and submerging the sensors fully in the pH buffer result in significantly better reproducibility. However, as can be seen from the figure the sensor is not very sensitive in the lower pH range. This could pose a challenge when the sensor would be implemented in the application

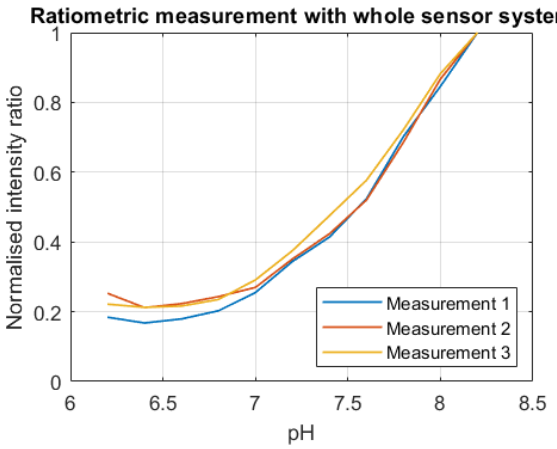

Figure 4.12: Measurements using the new fabricated pH buffers. Three measurements of the same sensor are shown

4.3.6. Sixth batch

In this section the results of the response time measurements, explained in Section 3.3.1, will be shown. In Figure 4.13, the result of the first and second response time measurement can be seen. In Figure 4.13a, the normalised intensity ratio is shown for an increase in pH value from 6.2 to 8.2. The red dotted line indicates the moment of the transfer from 6.2 to 8.2. In order to have standardised and comparable response time measurement, the time constant (τ) is calculated. This is done by using Equation 4.2. In this equation R is the response time curve, $R_{equilibrium}$ is the equilibrium value of the curve which as can be seen from the figure is approximately 0.9. Furthermore, $R_{initial}$ is the initial value of the measurement which is 0.72. By putting these values in Equation 4.2, the curve value at time τ can be calculated. Thereafter, using the curve the time constant can be found. Which is 43s as can be seen in Figure 4.13a.

$$R(\tau) = \frac{1}{e}(R_{equilibrium} - R_{initial}) + R_{initial} \tag{4.2}$$

The response time measurement of the sensor for decreasing pH can be seen in Figure 4.13b. The vertical red dotted line indicates the time of transfer from the 6.2 pH buffer to 8.2 pH buffer. The same time constant calculation can be done for this curve. This resulted in a time constant of 30s which is very fast. However, as can be seen from the Figure,it is not a good representation of response time of the sensor, since it takes the sensor more than 5 minutes to reach equilibrium.

4.4. Results Summary

In this section the results obtained in this work will be summarized in order to give a clear view of what has been accomplished. The objective of the first measurement was to see if the concept of the sensor layer worked. Therefore, a clear relation between the fluorescence emission and the pH value that is deposited on the sensor layer. As can be seen in the first result a clear relation between the pH and the fluorescence emission is shown, see Figure 4.1a and 4.1b. Furthermore, the response time of the sensor layer is depicted in Figure 4.2, where it can be seen that the response time is well below one minute.

In the first measurement only one 475nm LED was used. This is changed to two LEDs in the second measurement in order to implement ratiometric sensing. This is done by using one LED of 450nm and one of 405nm. It was hypothesized and also shown in literature [62], [85], [34], that by using a dual excitation single emission sensing scheme ratiometric sensing could be implemented. However, as shown in Figures 4.3 and 4.4, this was not the case. The fluorescence intensity of the sensor layer should decrease when the pH value would be increased when excited with the 405nm LED, but as can

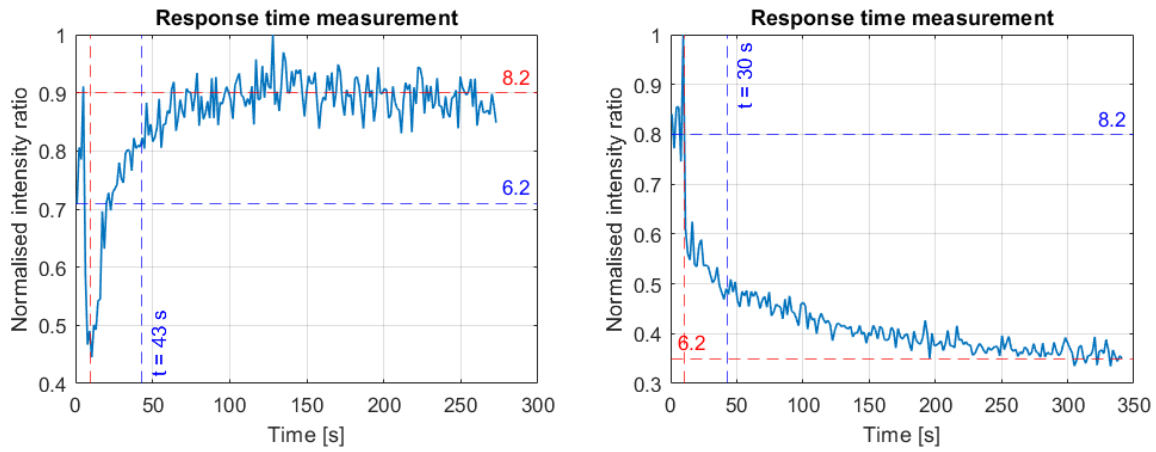

(a) Response time measurement with increasing pH

(b) Response time measurement with decreasing pH

Figure 4.13: Response time measurement with decreasing pH

be seen in the figure it increases. Therefore, a new dual excitation dual emission scheme was used which did give the desired result as can be seen in Figures 4.7a and 4.7.

After this the final sensor system was build and tested where the most challenging parameter was found to be the reproducibility. Several different measurements have been conducted to see how the reproducibility of the sensor layers could be improved. It was found that the combination of rinsing the produced HTPS loaded microbeads a few times to remove residual free HPTS molecules and submerging the whole sensor layer in the pH buffer solutions, yielded the best result as can be seen in Figure 4.12.

Lastly, the response time is measured. This resulted in a response time of less than a minute for increasing pH. However, for decreasing pH the response time is significantly higher with more than 5 minutes before equilibrium was reached.

In this Chapter various results have been obtained. The main challenges of these measurements were to improve the reproducibility and to find out why the sensor layers did not show the dual excitation/single emission behaviour which was expected from the material. These two aspects will be discussed in more detail in the next chapter.

5 Discussion

The objective of this thesis was to design a noninvasive sensor system with the objective to monitor the heart during the cardiac surgery and to detect changes in the health status of the heart tissue. As can be seen in previous chapters this objective is achieved by designing a prototype fluorescent pH sensor consisting of the following main components:

- **Sensor layer**: This layer consists of the fluorescence indicator dye 8- Hydroxypyrene-1,3,6-trisulfonic acid trisodium salt (HPTS) which is bonded to anion exchange resin beads. These microbeads are thereafter immobilized in a hydrogel support matrix, whereafter the layer deposited on thin glass using drop casting.
- **Optical system**: The system consists of two LEDs with two different wavelenghts, one at 405nm and the other at 450nm. Due to the dual excitation bands of HPTS ratiometric sensing could be implemented. The fluorescent emission of the sensor layer due to excitation by the LEDs was thereafter captured by an optical fibre which guided the signal to a spectrometer.
- **Data processor** The collected data from the spectrometer is thereafter processed with a computer. On this computer MATLAB is used to extract the peak emission on the specific wavelengths and the calculates the ratio.

With this design the main research objective has been achieved. However, by testing the designed sensor system some discrepancies and limitation were discovered. These will be elaborated and explained in this chapter. First the stated research questions in Chapter 1 will be answered, whereafter the measurement results will be discussed alongside with the discrepancies with literature and the discovered limitation will be explained. Lastly, recommendations for future research will be made.

5.1. Research questions revisited

The research questions state in Chapter 1 will be revisited and answered using the research conducted during this thesis.

RQ 1: What are the key principles of fluorescence sensing and how can they be used for measuring acidity of heart tissue?
As stated in Section 1.2, fluorescence is defined as the emission of visible light due to the absorption of photons by a certain molecules called fluorophores. These molecules absorb light of a certain wavelength and then emit it at a longer wavelength. These wavelengths are called the excitation and emission wavelengths respectively and are a material property. Other properties of fluorophores are there quantum yield and the fluorescence life time. Where the quantum yield is the ratio of between the absorbed and emitted photons, which is effectively the fluorescence efficiency. The fluorescence lifetime is the the average time the photons will spend on average in the excited state before it returns to the ground state accompanied with the emission of a photon. These properties can be utilized for fluorescence sensing of pH values due to the fact that certain fluorophores change their molecular structure when the acidity of their environment changes. This could result in a change in quantum yield and/or a change in fluorescence lifetime.

Several sensing schemes have been discussed in Section 1.4, including fluorescence intensity sensing, lifetime sensing and Förster resonance energy transfer (FRET). The choice was made to fluorescence intensity sensing, where the intensity of the fluorophore would change as a function of pH. This choice was made since this is the most simple sensing scheme and does not need complex electronics as opposed to lifetime sensing or two fluorophores and careful calibration which is needed for FRET.

RQ 2: What kind of materials are needed to produce the sensor layer?
The first type of material that is needed for the fabrication of the sensor layer is the fluorescent indicator dye. This is a material that alters its fluorescence properties when the acidity of the environment changes. In Section 2.2, several of these dyes have been listed of these indicator dyes Hydroxypyrene-1,3,6-trisulfonic acid trisodium salt (HPTS) was chosen for this application. This indicator dye has two excitation peaks one at 405nm and one at 460nm. By using both wavelengths ratiometric sensing is possible which increases the accuracy and stability of the measurements. Furthermore, it has a great sensitivity at near neutral pH values which is desired for this application. Other advantages of HTPS include: relatively low cost, non toxicity and high water solubility. However, the main disadvantage of this dye is the difficulty to immobilize it in support matrices. This immobilization in a support matrix is needed to provide stability flexibility and to prevent dye leaching.

Therefore, the method described Kermis [62] and Cattini [85] is used in this thesis. In these works the HPTS is bounded to anion exchange resin microbeads which can thereafter, be immobilized in a hydrogel support matrix.

RQ 3: How should the optical system be designed to ensure accurate measurement results and simplicity
The design of optical system is highly dependent on the properties of the sensor layer. Since in this work HPTS is used the optical system should be able to excite the sensor layer with two different wavelengths. Furthermore, it was found that the sensor layer did not exhibit the expected single emission band behaviour which is described in literature but dual emission bands. This finding will be discussed later in this chapter. Therefore, in order to implement ratiometric sensing, the optical system should be able to detect fluorescence emission of different wavelengths. Therefore, the choice was made to use a combination of an optical fibre and spectrometer as detector. This had the advantage that the whole spectrum could be analyzed which resulted in a more clear understanding of the behaviour of the sensor layer. Furthermore, since the whole spectrum is recorded and signal processing can be used no physical filters are needed. This significantly decreases the size, costs and complexity of the sensor system. As excitation sources two LEDs are used one of 405nm and one of 450nm which are able to excite both the protonated and deprotonated forms of HPTS respectively. The optical system and the glass slide on which the sensor layer was deposited, were placed in a 3D printed housing to form a small 2x2x2cm package.

5.2. Challenges

The main focus of this thesis has been to get a stable and reproducible sensor which meets the requirements set by a medical specialist in [84]. The measurement methods and results are shown in Chapter 3 and 4. Two of the aspects of these measurements results will be discussed in this section in more detail.

The first unexpected result that will be discussed is the result obtained in Section 4.2. In this section it was shown that the sensor layer did not shown the expected ratiometric behaviour. As described in Section 1.5.2, HTPS should have two excitation bands ,one around 405nm and around 450nm, and a single emission band at 510nm. It is shown in several works[64] [34] [62], that emission at 510nm should decrease with increasing pH when excited with 405nm and that the emission should increase with increasing pH when excited with 450nm. However, as can be seen in Figure 4.4 both emission increase with increasing pH which is opposite to the expected behaviour. In order to find out what the cause of this unexpected behaviour several tests have been performed. As can be seen in Section 3.2.3, the proportionality with pH of the sensor layer when excited with 405nm was not due to the use of microbeads and hydrogel. Furthermore, it was tested whether the supply current of the LED played a role in this behaviour but it was found out that this is not the case.

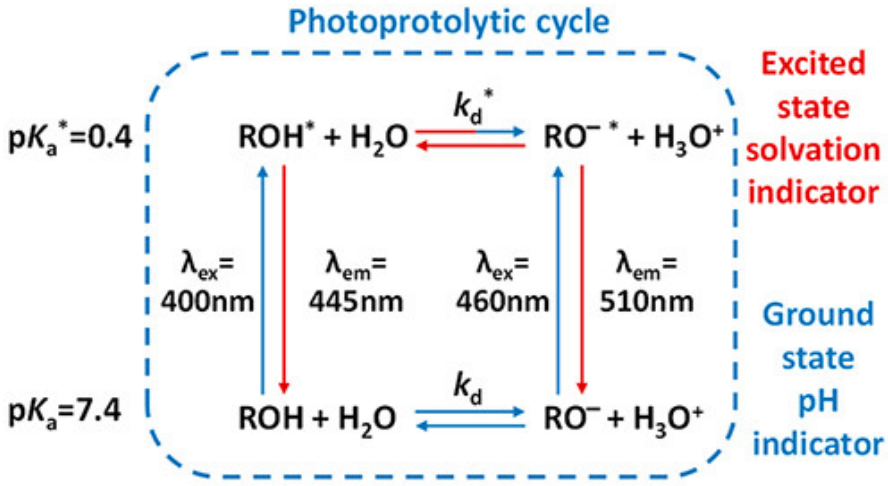

Figure 5.1: Fluorescence mechanisms of HPTS from [87]

The main hypothesis why this behaviour is shown is based on the work of Hakonen [86] and Nandi [87]. In these works the principle of the single vs dual emission bands of HPTS are discussed. It is said that in normal solutions HPTS has only one significant emission band. This is due to the fact that when ROH is illuminated with 405nm it will get excited and become ROH^*. Thereafter, in the excited state, proton transfer takes place which transforms ROH^* to RO^{-*} whereafter it relaxes to the ground state accompanied by the emission of a photon 510nm. So both the excitation of ROH and ROH^- results in the emission of 510nm. However, as is stated in [86] when HPTS is immobilized to a surface proton transfer in the excited stated is inhibited which means that the transition from ROH^* to RO^{-*} is less likely and the transition from ROH^* to ROH will be more likely. Therefore, in this case the emission of photons at 445nm will be more pronounced, see Figure 5.1. That is the reason why the dual excitation dual emission scheme can be used in this application. However, this does still not explain why the fluorescence emission of the sensor layer increases with increasing pH when excited with 405nm. This can be explained by the large excitation band of the sensor layer. This means that the UV LED does not only excite the protonated form of HPTS but also ´the deprotonated form. This result in the proportionality to pH which can be seen in Figure 4.4.

The second unexpected behaviour is the relatively poor reproducibility. This can mostly be attributed to the deformation of the sensor layer, which occurs upon contact with water solutions. This deformation which is not´the same for each measurement is most likely the result for the variability in the fluorescence emission of the sensor layer.

5.3. Recommendations

This thesis has delivered a sensor which is able to sense pH. However, before the sensor can be used some issues should be solved. In this sections the recommendation derived from this research will be stated.

Ionic strength: In this thesis the consequences of ionic strength have not been elaborated. This due to the fact that the main focus was on making a stable and reproducible sensor. Furthermore, the effects of ionic strength on the chosen indicator dye has been reported in earlier work [84]. Due to the fact that changes in ionic strength of the measurement environment can have significant consequences on the output of the sensor, this should be accounted for. The most simple method for this is to use a HPTS derivative called DPHDS which has one sulfonic group less which means it is less negatively charged which leads to a slight decrease in sensitivity to ionic strength [88]. Another way to compensate for the ionic strength is to conduct parallel conductive measurement to make an estimate of the ionic strength of the sample [64]. However, this would also be just an approximation.

pH range: As can be seen in Figure 4.12, the sensitivity of the sensor layer is not as desired for low

pH values. It can be seen that the sensor layer starts to show significant sensitivity from a pH value of 6.8. However, for the application of this thesis the lower ranges are also needed as well. In order to shift the pKa to the lower pH ranges, the concentration of HPTS can be altered [84]. Furthermore, the combination with another support matrix could also cause a shift in the pKa of the sensor layer. Lastly, other indicator dyes could be used with a lower intrinsic pKa.

Optical system: The current system uses two LEDs at different positions and an optical fibre leading to a spectrometer as detector. In order to make the system cheaper the detector could be replaced with photodiodes with optical filters attached to them in order to detect only the wavelengths in which the signal is present. Furthermore, the LEDs are now located in different places as can be seen in Figure 3.6. The fact that the light does therefore not reach the exact same location for each LED a slight difference in the fluorescence excitation and emission could occur. This could potentially have negative consequences for ratiometric sensing. This is due to the fact that the principle of ratiometric sensing should make the influence of non analyte specific factors such as detector orientation, indicator concentration and geometry of the sensor layer. However, if the LEDs that are used are not properly aligned this could result in the decrease in the effectiveness of ratiometric sensing. Therefore, in future work it should be examined if the LEDs could be coupled through an optical fibre in such a way that both the light sources point to the exact same area.

Support Matrix: As discussed in the previous section, the hydrogel support matrix shows significant deformation upon contact with water which results in variability in measurement result. Therefore in future work other support matrices should be examined. It was not done in this work since these support matrices have mostly a complicated fabrication process which is not the area of expertise of the author.

Combination pH and oxygen sensor: The work in this thesis will be continued by Dr. Avik Sett, who will incorporate the knowledge obtained in this research in a new sensor design which will be able to sense both pH and oxygen. This will be done by making a sensor layer which not only consists of the indicator dye HPTS but it will add ruthenium particles which shows fluorescence sensitivity to oxygen. The challenges that needs to be faced are that special care must be taken to ensure no cross sensitivity occurs between the two indicator dye. Furthermore, it should be examined which support matrix is able to hold both of the indicator dyes.

5.4. Conclusions

In this work a fluorescence pH sensor is designed and fabricated. The measurement result show a good relation between the emission ratio and the pH since a five fold increase can be seen in the emission ratio over pH range of 6.2-8.2. This was achieved by using a dual-excitation/dual-emission ratiometric sensing scheme. Furthermore, the response time is significantly improved when compared to the work described in [84]. However, for future work the reproducibility of the sensor system could be improved by working with different materials for the support matrix. Furthermore, to ensure the sensor would work for the intended application, it should be tested on actual tissue. This was not done during this thesis due to time constraints. Lastly, the combination with the oxygen sensor which will be implemented in the work of Dr. Sett, would give a significantly better view of the health status of the heart tissue.

References

[1] N. H. Lung and B. Institute. (Jun. 2022), [Online]. Available: https://www.nhlbi.nih.gov/health/heart-surgery#:~:text=Each%20year%2C%20more%20than%202,ages%20can%20have%20heart%20surgery..

[2] N. Koning, "Protection of the microcirculation during cardiac surgery with cardiopulmonary bypass," English, Ph.D. dissertation, Vrije Universiteit Amsterdam, 2017, ISBN: 9789462336162.

[3] M. Sarkar and V. Prabhu, "Basics of cardiopulmonary bypass," en, *Indian J Anaesth*, vol. 61, no. 9, pp. 760–767, Sep. 2017.

[4] J. M. Ali, L. F. Miles, Y. Abu-Omar, C. Galhardo, and F. Falter, "Global cardioplegia practices: Results from the global cardiopulmonary bypass survey," en, *J Extra Corpor Technol*, vol. 50, no. 2, pp. 83–93, Jun. 2018.

[5] Y. Fan, A.-M. Zhang, Y.-B. Xiao, Y.-G. Weng, and R. Hetzer, "Warm versus cold cardioplegia for heart surgery: a meta-analysis," *European Journal of Cardio-Thoracic Surgery*, vol. 37, no. 4, pp. 912–919, Apr. 2010, ISSN: 1010-7940. DOI: 10.1016/j.ejcts.2009.09.030. eprint: https://academic.oup.com/ejcts/article-pdf/37/4/912/17790764/37-4-912.pdf. [Online]. Available: https://doi.org/10.1016/j.ejcts.2009.09.030.

[6] M.-M. Gebhard, H. J. Bretschneider, and P. A. Schnabel, "Cardioplegia principles and problems," in *Physiology and pathophysiology of the heart*, Springer, 1989, pp. 655–668.

[7] P. Voci, F. Bilotta, Q. Caretta, F. Chiarotti, C. Mercanti, and B. Marino, "Mechanisms of Incomplete Cardioplegia Distribution during Coronary Artery Surgery: An Intraoperative Transesophageal Contrast Echocardiography Study," *Anesthesiology*, vol. 79, no. 5, pp. 904–912, Nov. 1993, ISSN: 0003-3022. DOI: 10.1097/00000542-199311000-00006. eprint: https://pubs.asahq.org/anesthesiology/article-pdf/79/5/904/644556/0000542-199311000-00006.pdf. [Online]. Available: https://doi.org/10.1097/00000542-199311000-00006.

[8] C. Preusse, M. Gebhard, and H. Bretschneider, "Interstitial ph value in the myocardium as indicator of ischemic stress of cardioplegically arrested hearts," *Basic Research in Cardiology*, vol. 77, pp. 372–387, 1982.

[9] F. J. Walters, G. J. Wilson, D. J. Steward, R. J. Domenech, and D. C. MacGregor, "Intramyocardial ph as an index of myocardial metabolism during cardiac surgery," *The Journal of Thoracic and Cardiovascular Surgery*, vol. 78, no. 3, pp. 319–330, 1979, ISSN: 0022-5223. DOI: https://doi.org/10.1016/S0022-5223(19)38098-5. [Online]. Available: https://www.sciencedirect.com/science/article/pii/S0022522319380985.

[10] T. C. Axford, J. A. Dearani, I. Khait, *et al.*, "Electrode-derived myocardial ph measurements reflect intracellular myocardial metabolism assessed by phosphorus 31-nuclear magnetic resonance spectroscopy during normothermic ischemia," *The Journal of Thoracic and Cardiovascular Surgery*, vol. 103, no. 5, pp. 902–907, 1992, ISSN: 0022-5223. DOI: https://doi.org/10.1016/S0022-5223(19)34914-1. [Online]. Available: https://www.sciencedirect.com/science/article/pii/S0022522319349141.

[11] B. Senst, A. Kumar, and R. R. Diaz, "Cardiac surgery," en, in *StatPearls*, Treasure Island (FL): StatPearls Publishing, Jan. 2023.

[12] N. Ahmed, "Chapter 2 - myocardial ischemia," in *Pathophysiology of Ischemia Reperfusion Injury and Use of Fingolimod in Cardioprotection*, N. Ahmed, Ed., Academic Press, 2019, pp. 41–56, ISBN: 978-0-12-818023-5. DOI: https://doi.org/10.1016/B978-0-12-818023-5.00002-9. [Online]. Available: https://www.sciencedirect.com/science/article/pii/B9780128180235000029.

[13] R. B. Jennings and K. A. Reimer, "The cell biology of acute myocardial ischemia," en, *Annu Rev Med*, vol. 42, pp. 225–246, 1991.

[14] P. Neupane, S. Bhuju, N. Thapa, and H. K. Bhattarai, *Biomolecular Concepts*, vol. 10, no. 1, pp. 1–10, 2019. DOI: doi:10.1515/bmc-2019-0001. [Online]. Available: https://doi.org/10.1515/bmc-2019-0001.

[15] W. C. Stanley, "Myocardial energy metabolism during ischemia and the mechanisms of metabolic therapies," *Journal of Cardiovascular Pharmacology and Therapeutics*, vol. 9, no. 1_suppl, S31–S45, 2004, PMID: 15378130. DOI: 10.1177/107424840400900104. eprint: https://doi.org/10.1177/107424840400900104. [Online]. Available: https://doi.org/10.1177/107424840400900104.

[16] J. Borges and M. Lessa, "Mechanisms involved in exercise-induced cardioprotection: A systematic review," *Arquivos brasileiros de cardiologia*, vol. 105, Mar. 2015. DOI: 10.5935/abc.20150024.

[17] S. Verma, P. W. Fedak, R. D. Weisel, *et al.*, "Fundamentals of reperfusion injury for the clinical cardiologist," *Circulation*, vol. 105, no. 20, pp. 2332–2336, 2002. DOI: 10.1161/01.CIR.0000016602.96363.36. eprint: https://www.ahajournals.org/doi/pdf/10.1161/01.CIR.0000016602.96363.36. [Online]. Available: https://www.ahajournals.org/doi/abs/10.1161/01.CIR.0000016602.96363.36.

[18] Hoffman, John W., Gilbert, Timothy B., Poston, Robert S., and Silldorff, Erik P., "Myocardial reperfusion injury: Etiology, mechanisms, and therapies," *J Extra Corpor Technol*, vol. 36, no. 4, pp. 391–411, 2004. DOI: 10.1051/ject/2004364391. [Online]. Available: https://doi.org/10.1051/ject/2004364391.

[19] D. J. Hausenloy and D. M. Yellon, "Myocardial ischemia-reperfusion injury: A neglected therapeutic target," en, *J Clin Invest*, vol. 123, no. 1, pp. 92–100, Jan. 2013.

[20] J. Bradić, M. Andjić, J. Novaković, N. Jeremić, and V. Jakovljević, "Cardioplegia in open heart surgery: Age matters," *Journal of Clinical Medicine*, vol. 12, no. 4, 2023, ISSN: 2077-0383. DOI: 10.3390/jcm12041698. [Online]. Available: https://www.mdpi.com/2077-0383/12/4/1698.

[21] C. Carvajal, A. Goyal, and P. Tadi, *Cardioplegia*. StatPearls Publishing, Treasure Island (FL), 2023. [Online]. Available: http://europepmc.org/books/NBK554463.

[22] D. J. Chambers and H. B. Fallouh, "Cardioplegia and cardiac surgery: Pharmacological arrest and cardioprotection during global ischemia and reperfusion," *Pharmacology & Therapeutics*, vol. 127, no. 1, pp. 41–52, 2010, ISSN: 0163-7258. DOI: https://doi.org/10.1016/j.pharmthera.2010.04.001. [Online]. Available: https://www.sciencedirect.com/science/article/pii/S0163725810000732.

[23] "Characteristics of fluorescence emission," in *Molecular Fluorescence*. John Wiley & Sons, Ltd, 2012, ch. 3, pp. 53–74, ISBN: 9783527650002. DOI: https://doi.org/10.1002/9783527650002.ch3. eprint: https://onlinelibrary.wiley.com/doi/pdf/10.1002/9783527650002.ch3. [Online]. Available: https://onlinelibrary.wiley.com/doi/abs/10.1002/9783527650002.ch3.

[24] "Introduction to fluorescence," in *Principles of Fluorescence Spectroscopy*, J. R. Lakowicz, Ed. Boston, MA: Springer US, 2006, pp. 1–26, ISBN: 978-0-387-46312-4. DOI: 10.1007/978-0-387-46312-4_1. [Online]. Available: https://doi.org/10.1007/978-0-387-46312-4_1.

[25] *Fluorescence and phosphorescence*, [Online; accessed 2024-04-24], Jan. 2023. [Online]. Available: https://chem.libretexts.org/@go/page/41400.

[26] S. Draxler, "Lifetime based sensors / sensing," in *Advanced Concepts in Fluorescence Sensing: Part B: Macromolecular Sensing*, C. D. Geddes and J. R. Lakowicz, Eds. Boston, MA: Springer US, 2005, pp. 241–274, ISBN: 978-0-387-23647-6. DOI: 10.1007/0-387-23647-3_8. [Online]. Available: https://doi.org/10.1007/0-387-23647-3_8.

[27] S. b. Granite, *Stokes shift, fluorescence spectroscopy*, Feb. 2023. [Online]. Available: https://www.edinst.com/blog/what-is-the-stokes-shift/.

[28] "Quenching," 2019. DOI: doi:10.1351/goldbook.Q05007. [Online]. Available: https://doi.org/10.1351/goldbook.Q05007.

[29] S. Doose, H. Neuweiler, and M. Sauer, “Fluorescence quenching by photoinduced electron transfer: A reporter for conformational dynamics of macromolecules,” *ChemPhysChem*, vol. 10, no. 9-10, pp. 1389–1398, 2009. DOI: https://doi-org.tudelft.idm.oclc.org/10.1002/cphc.200900238. eprint: https://chemistry-europe-onlinelibrary-wiley-com.tudelft.idm.oclc.org/doi/pdf/10.1002/cphc.200900238. [Online]. Available: https://chemistry-europe-onlinelibrary-wiley-com.tudelft.idm.oclc.org/doi/abs/10.1002/cphc.200900238.

[30] M. Verma, A. F. Chaudhry, and C. J. Fahrni, “Predicting the photoinduced electron transfer thermodynamics in polyfluorinated 1, 3, 5-triarylpyrazolines based on multiple linear free energy relationships,” *Organic & biomolecular chemistry*, vol. 7, no. 8, pp. 1536–1546, 2009.

[31] H. Niu, J. Liu, H. M. O’Connor, T. Gunnlaugsson, T. D. James, and H. Zhang, “Photoinduced electron transfer (pet) based fluorescent probes for cellular imaging and disease therapy,” *Chem. Soc. Rev.*, vol. 52, pp. 2322–2357, 7 2023. DOI: 10.1039/D1CS01097B. [Online]. Available: http://dx.doi.org/10.1039/D1CS01097B.

[32] A. Steinegger and S. Borisov, “Optical sensing and imaging of ph values: Spectroscopies, materials and applications,” *Chemical Reviews*, vol. 120, pp. 12 357–12 489, Dec. 2020. DOI: 10.1021/acs.chemrev.0c00451.

[33] C. G. Frankaer, K. J. Hussain, T. C. Dorge, and T. J. Sørensen, “Optical chemical sensor using intensity ratiometric fluorescence signals for fast and reliable ph determination,” *ACS sensors*, vol. 4, no. 1, pp. 26–31, 2018.

[34] S. Ulrich, A. Osypova, G. Panzarasa, R. M. Rossi, N. Bruns, and L. F. Boesel, “Pyranine-modified amphiphilic polymer conetworks as fluorescent ratiometric ph sensors,” *Macromolecular Rapid Communications*, vol. 40, no. 21, p. 1 900 360, 2019. DOI: https://doi-org.tudelft.idm.oclc.org/10.1002/marc.201900360. eprint: https://onlinelibrary-wiley-com.tudelft.idm.oclc.org/doi/pdf/10.1002/marc.201900360. [Online]. Available: https://onlinelibrary-wiley-com.tudelft.idm.oclc.org/doi/abs/10.1002/marc.201900360.

[35] N. Boens, W. Qin, N. Basarić, A. Orte, E. M. Talavera, and J. M. Alvarez-Pez, “Photophysics of the fluorescent ph indicator bcecf,” *The Journal of Physical Chemistry A*, vol. 110, no. 30, pp. 9334–9343, 2006.

[36] K. Suhling, L. M. Hirvonen, J. A. Levitt, *et al.*, “Fluorescence lifetime imaging (flim): Basic concepts and some recent developments,” *Medical photonics*, vol. 27, pp. 3–40, 2015.

[37] X.-d. Wang and O. S. Wolfbeis, “Optical methods for sensing and imaging oxygen: Materials, spectroscopies and applications,” *Chem. Soc. Rev.*, vol. 43, pp. 3666–3761, 10 2014. DOI: 10.1039/C4CS00039K. [Online]. Available: http://dx.doi.org/10.1039/C4CS00039K.

[38] A. S. Vasylevska, A. A. Karasyov, S. M. Borisov, and C. Krause, “Novel coumarin-based fluorescent ph indicators, probes and membranes covering a broad ph range,” *Analytical and bioanalytical chemistry*, vol. 387, pp. 2131–2141, 2007.

[39] C.-G. Niu, X.-Q. Gui, G.-M. Zeng, and X.-Z. Yuan, “A ratiometric fluorescence sensor with broad dynamic range based on two ph-sensitive fluorophores,” *Analyst*, vol. 130, no. 11, pp. 1551–1556, 2005.

[40] F. Le Guern, V. Mussard, A. Gaucher, M. Rottman, and D. Prim, “Fluorescein derivatives as fluorescent probes for ph monitoring along recent biological applications,” *International Journal of Molecular Sciences*, vol. 21, no. 23, 2020, ISSN: 1422-0067. DOI: 10.3390/ijms21239217. [Online]. Available: https://www.mdpi.com/1422-0067/21/23/9217.

[41] F. Le Guern, V. Mussard, A. Gaucher, M. Rottman, and D. Prim, “Fluorescein derivatives as fluorescent probes for ph monitoring along recent biological applications,” *International Journal of Molecular Sciences*, vol. 21, no. 23, p. 9217, 2020.

[42] M. M. Martin and L. Lindqvist, “The ph dependence of fluorescein fluorescence,” *Journal of Luminescence*, vol. 10, no. 6, pp. 381–390, 1975.

[43] M. Bennet, “Multi-parameter quantitative mapping of microfluidic devices,” Ph.D. dissertation, Jan. 2011.

[44] L. Tang, L. Zhu, Y. Wang, and C. Fang, “Uncovering the hidden excited state toward fluorescence of an intracellular ph indicator,” *The Journal of Physical Chemistry Letters*, vol. 9, no. 17, pp. 4969–4975, 2018.

[45] A. Chandra, S. Prasad, H. Iuele, *et al.*, “Highly sensitive fluorescent ph microsensors based on the ratiometric dye pyranine immobilized on silica microparticles,” *Chemistry – A European Journal*, vol. 27, no. 53, pp. 13 318–13 324, 2021. DOI: https://doi-org.tudelft.idm.oclc.org/10.1002/chem.202101568. eprint: https://chemistry-europe-onlinelibrary-wiley-com.tudelft.idm.oclc.org/doi/pdf/10.1002/chem.202101568. [Online]. Available: https://chemistry-europe-onlinelibrary-wiley-com.tudelft.idm.oclc.org/doi/abs/10.1002/chem.202101568.

[46] R. Kumar, R. Yadav, M. A. Kolhe, R. S. Bhosale, and R. Narayan, “8-hydroxypyrene-1,3,6-trisulfonic acid trisodium salt (hpts) based high fluorescent, ph stimuli waterborne polyurethane coatings,” *Polymer*, vol. 136, pp. 157–165, 2018, ISSN: 0032-3861. DOI: https://doi.org/10.1016/j.polymer.2017.12.056. [Online]. Available: https://www.sciencedirect.com/science/article/pii/S0032386117312284.

[47] O. S. Wolfbeis, E. Fürlinger, H. Kroneis, and H. Marsoner, “Fluorimetrische analyse: 1. a study on fluorescent indicators for measuring near neutral (“physiological”) ph-values,” *Fresenius’ Zeitschrift fuer Analytische Chemie*, vol. 314, pp. 119–124, 1983.

[48] J. Han and K. Burgess, “Fluorescent indicators for intracellular ph,” *Chemical reviews*, vol. 110, no. 5, pp. 2709–2728, 2010.

[49] J. E. Whitaker, R. P. Haugland, and F. G. Prendergast, “Spectral and photophysical studies of benzo [c] xanthene dyes: Dual emission ph sensors,” *Analytical biochemistry*, vol. 194, no. 2, pp. 330–344, 1991.

[50] S. Mordon, J. Devoisselle, and S. Soulié, “Fluorescence spectroscopy of ph in vivo using a dual-emission fluorophore (c-snafl-1),” *Journal of Photochemistry and Photobiology B: Biology*, vol. 28, no. 1, pp. 19–23, 1995, ISSN: 1011-1344. DOI: https://doi.org/10.1016/1011-1344(94)07100-3. [Online]. Available: https://www.sciencedirect.com/science/article/pii/1011134494071003.

[51] D. Wencel, T. Abel, and C. McDonagh, “Optical chemical ph sensors,” *Analytical Chemistry*, vol. 86, no. 1, pp. 15–29, 2014, PMID: 24180284. DOI: 10.1021/ac4035168. eprint: https://doi.org/10.1021/ac4035168. [Online]. Available: https://doi.org/10.1021/ac4035168.

[52] N. De Acha, C. Elosua, I. Matias, and F. J. Arregui, “Luminescence-based optical sensors fabricated by means of the layer-by-layer nano-assembly technique,” *Sensors*, vol. 17, no. 12, 2017, ISSN: 1424-8220. DOI: 10.3390/s17122826. [Online]. Available: https://www.mdpi.com/1424-8220/17/12/2826.

[53] B. D. MacCraith and C. McDonagh, “Enhanced fluorescence sensing using sol-gel materials,” *Journal of Fluorescence*, vol. 12, pp. 333–342, 2002.

[54] T. Nguyen, K. P. McNamara, and Z. Rosenzweig, “Optochemical sensing by immobilizing fluorophore-encapsulating liposomes in sol–gel thin films,” *Analytica Chimica Acta*, vol. 400, no. 1, pp. 45–54, 1999, ISSN: 0003-2670. DOI: https://doi.org/10.1016/S0003-2670(99)00607-8. [Online]. Available: https://www.sciencedirect.com/science/article/pii/S0003267099006078.

[55] O. Guillermo, M. C. Moreno-Bondi, D. Garcia-Fresnadillo, and M. D. Marazuela, “The interplay of indicator, support and analyte in optical sensor layers,” in *Frontiers in Chemical Sensors: Novel Principles and Techniques*, G. Orellana and M. C. Moreno-Bondi, Eds. Berlin, Heidelberg: Springer Berlin Heidelberg, 2005, pp. 189–225, ISBN: 978-3-540-27757-6. DOI: 10.1007/3-540-27757-9_6. [Online]. Available: https://doi.org/10.1007/3-540-27757-9_6.

[56] J. M. Rosiak and F. Yoshii, “Hydrogels and their medical applications,” *Nuclear Instruments and Methods in Physics Research Section B: Beam Interactions with Materials and Atoms*, vol. 151, no. 1, pp. 56–64, 1999, ISSN: 0168-583X. DOI: https://doi.org/10.1016/S0168-583X(99)00118-4. [Online]. Available: https://www.sciencedirect.com/science/article/pii/S0168583X99001184.

[57] S. K. H. Gulrez, S. Al-Assaf, and G. O. Phillips, “Hydrogels: Methods of preparation, characterisation and applications,” in *Progress in Molecular and Environmental Bioengineering*, A. Carpi, Ed., Rijeka: IntechOpen, 2011, ch. 5. DOI: 10.5772/24553. [Online]. Available: https://doi.org/10.5772/24553.

[58] Y. Dahman, “Chapter 3 - smart nanomaterials**by yaser dahman, adil kamil, and daniel baena.,” Micro and Nano Technologies, Y. Dahman, Ed., pp. 47–66, 2017. DOI: https://doi.org/10.1016/B978-0-323-51256-5.00003-4. [Online]. Available: https://www.sciencedirect.com/science/article/pii/B9780323512565000034.

[59] E. Alveroglu, A. Gelir, and Y. Yilmaz, “Swelling behavior of chemically ion-doped hydrogels,” *Macromolecular Symposia*, vol. 281, no. 1, pp. 174–180, 2009. DOI: https://doi.org/10.1002/masy.200950723. eprint: https://onlinelibrary.wiley.com/doi/pdf/10.1002/masy.200950723. [Online]. Available: https://onlinelibrary.wiley.com/doi/abs/10.1002/masy.200950723.

[60] B. M. Weidgans, C. Krause, I. Klimant, and O. S. Wolfbeis, “Fluorescent ph sensors with negligible sensitivity to ionic strength,” *Analyst*, vol. 129, no. 7, pp. 645–650, 2004.

[61] A. Tamayol, M. Akbari, Y. Zilberman, *et al.*, “Flexible ph-sensing hydrogel fibers for epidermal applications,” *Advanced Healthcare Materials*, vol. 5, no. 6, pp. 711–719, 2016. DOI: https://doi.org/10.1002/adhm.201500553. eprint: https://onlinelibrary.wiley.com/doi/pdf/10.1002/adhm.201500553. [Online]. Available: https://onlinelibrary.wiley.com/doi/abs/10.1002/adhm.201500553.

[62] H. R. Kermis, Y. Kostov, P. Harms, and G. Rao, “Dual excitation ratiometric fluorescent ph sensor for noninvasive bioprocess monitoring: Development and application,” *Biotechnology Progress*, vol. 18, no. 5, pp. 1047–1053, 2002. DOI: https://doi.org/10.1021/bp0255560. eprint: https://aiche.onlinelibrary.wiley.com/doi/pdf/10.1021/bp0255560. [Online]. Available: https://aiche.onlinelibrary.wiley.com/doi/abs/10.1021/bp0255560.

[63] C. McDonagh, B. MacCraith, and A. McEvoy, “Tailoring of sol- gel films for optical sensing of oxygen in gas and aqueous phase,” *Analytical chemistry*, vol. 70, no. 1, pp. 45–50, 1998.

[64] D. Wencel, B. MacCraith, and C. McDonagh, “High performance optical ratiometric sol–gel-based ph sensor,” *Sensors and Actuators B: Chemical*, vol. 139, no. 1, pp. 208–213, 2009.

[65] S. A. Grant and R. S. Glass, “A sol–gel based fiber optic sensor for local blood ph measurements,” *Sensors and Actuators B: Chemical*, vol. 45, no. 1, pp. 35–42, 1997.

[66] Mar. 2023. [Online]. Available: https://ibsen.com/technologies/fluorescence-spectroscopy/how-to-build-a-fluorometer/.

[67] *Fluorescence light sources: A comparative guide*. [Online]. Available: https://www.scientifica.uk.com/learning-zone/choosing-the-best-light-source-for-your-experiment#:~:text=Commonly%20used%20light%20sources%20in,lamps%20or%20tungsten%2Dhalogen%20lamps..

[68] Y.-H. Shin, M. T. Gutierrez-Wing, and J.-W. Choi, “Review—recent progress in portable fluorescence sensors,” *Journal of The Electrochemical Society*, vol. 168, no. 1, p. 017 502, Jan. 2021. DOI: 10.1149/1945-7111/abd494. [Online]. Available: https://dx.doi.org/10.1149/1945-7111/abd494.

[69] V. K. J. Darshan Chikkanayakanahalli Mukunda and K. K. Mahato, “Light emitting diodes (leds) in fluorescence-based analytical applications: A review,” *Applied Spectroscopy Reviews*, vol. 57, no. 1, pp. 1–38, 2022. DOI: 10.1080/05704928.2020.1835939. eprint: https://doi.org/10.1080/05704928.2020.1835939. [Online]. Available: https://doi.org/10.1080/05704928.2020.1835939.

[70] K. Aswani, T. Jinadasa, and C. M. Brown, “Fluorescence microscopy light sources,” *Microscopy Today*, vol. 20, no. 4, pp. 22–28, 2012. DOI: 10.1017/S1551929512000399.

[71] A. P. Demchenko, “The sensing devices,” in *Introduction to Fluorescence Sensing*. Cham: Springer International Publishing, 2015, pp. 507–550, ISBN: 978-3-319-20780-3. DOI: 10.1007/978-3-319-20780-3_11. [Online]. Available: https://doi.org/10.1007/978-3-319-20780-3_11.

[72] P. Magnan, “Detection of visible photons in ccd and cmos: A comparative view,” *Nuclear Instruments and Methods in Physics Research Section A: Accelerators, Spectrometers, Detectors and Associated Equipment*, vol. 504, no. 1-3, pp. 199–212, 2003.

[73] S. A. Taylor *et al.*, “Ccd and cmos imaging array technologies: Technology review,” *UK: Xerox Research Centre Europe*, pp. 1–14, 1998.

[74] Z. Yang, T. Albrow-Owen, W. Cai, and T. Hasan, “Miniaturization of optical spectrometers,” *Science*, vol. 371, no. 6528, eabe0722, 2021. DOI: 10.1126/science.abe0722. eprint: https://www.science.org/doi/pdf/10.1126/science.abe0722. [Online]. Available: https://www.science.org/doi/abs/10.1126/science.abe0722.

[75] M.-A. Serrano, J. Baró, J.-C. Esteve, and F.-J. García-Diego, “Spectral relative attenuation of solar radiation through a skylight focused on preventive conservation: Museo de l’almoina in valencia (spain) case study,” *Sensors*, vol. 21, p. 4651, Jul. 2021. DOI: 10.3390/s21144651.

[76] J. Reichman, “Handbook of optical filters for fluorescence microscopy,” *Chroma Technology Corporation*, 2000.

[77] J. W. Lichtman and J.-A. Conchello, “Fluorescence microscopy,” *Nature methods*, vol. 2, no. 12, pp. 910–919, 2005.

[78] [Online]. Available: https://www.chroma.com/support/knowledge-center/about-fluorescence/fluorescence-filter-types.

[79] Z. Li, N. Lan, Z. Cheng, *et al.*, “In vivo fiber-optic fluorescent sensor for real-time ph monitoring of tumor microenvironment,” *Chemical Engineering Journal*, vol. 493, p. 152 495, 2024, ISSN: 1385-8947. DOI: https://doi.org/10.1016/j.cej.2024.152495. [Online]. Available: https://www.sciencedirect.com/science/article/pii/S1385894724039822.

[80] Z. Bian, C. Dai, F. Chu, *et al.*, “Ph biosensors based on hydrogel optical fiber,” *Appl. Opt.*, vol. 62, no. 31, pp. 8272–8278, Nov. 2023. DOI: 10.1364/AO.501549. [Online]. Available: https://opg.optica.org/ao/abstract.cfm?URI=ao-62-31-8272.

[81] J. Gong, S. Venkateswaran, M. G. Tanner, J. M. Stone, and M. Bradley, “Polymer microarrays for the discovery and optimization of robust optical-fiber-based ph sensors,” *ACS Combinatorial Science*, vol. 21, no. 5, pp. 417–424, 2019.

[82] J. Gong, M. G. Tanner, S. Venkateswaran, J. M. Stone, Y. Zhang, and M. Bradley, “A hydrogel-based optical fibre fluorescent ph sensor for observing lung tumor tissue acidity,” *Analytica Chimica Acta*, vol. 1134, pp. 136–143, 2020, ISSN: 0003-2670. DOI: https://doi.org/10.1016/j.aca.2020.07.063. [Online]. Available: https://www.sciencedirect.com/science/article/pii/S0003267020308011.

[83] K. Huo, J. Zhang, T. Lin, Y. Zhang, Y. Liu, and X. Liu, “Colorimetric and fluorescent dual-mode ph sensor with pmia as substrate and cqds as probe for high accuracy detection of full range ph,” *Dyes and Pigments*, vol. 219, p. 111 574, 2023, ISSN: 0143-7208. DOI: https://doi.org/10.1016/j.dyepig.2023.111574. [Online]. Available: https://www.sciencedirect.com/science/article/pii/S0143720823005004.

[84] M. Vriesendorp, “Detecting myocardial ischaemia with optochemical sensing by using a fluorescent hydrogel,” MSc thesis, Delft University of Technology, Delft, NL, Aug. 2022.

[85] S. Cattini, L. Accorsi, S. Truzzi, and L. Rovati, “On the development of an instrument for in-line and real-time monitoring of blood-ph in extracorporeal circulation,” *IEEE Transactions on Instrumentation and Measurement*, vol. 69, no. 8, pp. 5640–5648, 2020. DOI: 10.1109/TIM.2019.2961499.

[86] A. Hakonen and S. Hulth, “A high-precision ratiometric fluorosensor for ph: Implementing time-dependent non-linear calibration protocols for drift compensation,” *Analytica Chimica Acta*, vol. 606, no. 1, pp. 63–71, 2008, ISSN: 0003-2670. DOI: https://doi.org/10.1016/j.aca.2007.10.035. [Online]. Available: https://www.sciencedirect.com/science/article/pii/S0003267007017795.

[87] R. Nandi and N. Amdursky, “The dual use of the pyranine (hpts) fluorescent probe: A ground-state ph indicator and an excited-state proton transfer probe,” *Accounts of Chemical Research*, vol. 55, no. 18, pp. 2728–2739, 2022.

[88] A. Hakonen and S. Hulth, “A high-performance fluorosensor for ph measurements between 6 and 9,” *Talanta*, vol. 80, no. 5, pp. 1964–1969, 2010, ISSN: 0039-9140. DOI: https://doi.org/10.1016/j.talanta.2009.10.055. [Online]. Available: https://www.sciencedirect.com/science/article/pii/S0039914009008443.

A

Matlab scripts

A.1. Code for plotting the data obtained from Oceanview

```
1
2  folder = "2ledsFirstUP";
3
4  fileNameblue = '*475*';
5  fileNameUv = '*405*';
6  wavelength = 520;
7  wavelength_uv = 435;
8  blue = dir(fullfile(folder,fileNameblue));
9  uv = dir(fullfile(folder,fileNameUv));
10 peaksblue = zeros(1,length(uv));
11 peaksUV_450 = zeros(1,length(uv));
12 pH_values = [6.2 6.6 7 7.4 7.8 8.2];
13
14 for i = 1:length(peaksblue)
15     peaksblue(i) = findWavelength(wavelength,table2array(readtable(
           fullfile(folder,blue(i).name),'decimal',',')));
16     peaksUV_450(i) = findWavelength(wavelength_blue,table2array(readtable(
           fullfile(folder,uv(i).name),'decimal',',')));
17 end
18
19 x0=10;
20 y0=10;
21 width=400;
22 height=300;
23 set(gcf,'position',[x0,y0,width,height])
24
25 ratio = peaksblue./peaksUV_450;
26
27 [f, gof] = fit(pH_values(:), ratioblue(:), 'logistic4');
28 plot(f, pH_values, ratioblue);
29 xlabel("pH");
30 ylabel("Intensity ratio");
31 grid on;
32 % legend("Location","southeast");
33 title("Ratiometric measurement");
```

A.2. Plotting response time from data obtained from Oceanview

```
1
2  close all;
3  files = dir('*txt*');
4  sortfiles = natsortfiles(files);
5  data = cell(1,length(sortfiles));
6  peaks = zeros(1,length(sortfiles));
7  wavelength = 515;
8  portion = 3;
9  tot_time = 0.5*length(sortfiles)/portion; %time in seconds when every 0.5s
       a file is generated
10 time = linspace(0,tot_time,(length(sortfiles)/portion));
11
12 x0=10;
13 y0=10;
14 width=400;
15 height=300;
16 set(gcf,'position',[x0,y0,width,height])
17 for i=1:length(sortfiles)
18     % data{i} = table2array(readtable(sortfiles(i).name,'decimal',','));
19
20     data{i} = table2array(readtable(sortfiles(i).name));
21     peaks(i) = findWavelength(wavelength,data{i});
22 end
23 normpeaks = peaks./max(peaks);
24 halfpeaks = normpeaks(1:length(normpeaks)/portion);
25 [f, gof] = fit(time(:),halfpeaks(:),'gompertz');
26 plot(f,time,halfpeaks);
27 xline(20,"--r",{"t = 20"})
28 grid on;
29 xlabel("Time [s]");
30 ylabel("Normalised intensity");
31 title("Response time measurement ")
32 legend("Location","southeast");
```

A.3. Plotting full spectra

```
1
2  % close all;
3  files = dir('*uv*');
4  fileNameUv = '*405*';
5   uv = dir(fileNameUv);
6  data = cell(1,length(uv));
7   ulegend = ["6.2","6.6","7.0","7.4", "7.8","8.2"];
8  newLegend = ["6.2 405nm","6.2 475nm","6.6 405nm","6.6 475nm","7.0 405nm
       ","7.0 475nm","7.4 405nm","7.4 475nm","7.8 405nm","7.8 475nm","8.2 405
       nm","8.2 475nm"];
9  x0=10;
10 y0=10;
11 width=400;
12 height=300;
13 set(gcf,'position',[x0,y0,width,height])
14
15
16
17 for i=1:length(files)
18     % data{i} = table2array(readtable(files(i).name,'decimal',','));
19     % Oceanviewdata
20      data{i} = table2array(readtable(files(i).name));
21      %matlab data
22
23     x = data{1,i}(50:800,1);
24     y = data{1,i}(50:800,2);
25
26     plot(x,y,"LineWidth",1);
27     hold on;
28 end
29 legend(ulegend,Location="northeast");
30 grid on;
31 xlabel("Wavelength [nm]");
32 ylabel("Measured intensity [counts]");
33 title("Spectrum of fluorescence emission")
```

A.4. Script for controlling the spectrometer and the LEDs

```
% close all;
sensor = '_2';
ph_value = '8_2';
%% connect to spectrometer and LED controller
port = 'COM20';
s = serialport(port,115200);
flame = icdevice('OceanOptics_OmniDriver.mdd');
connect(flame);

%% initialize spectrum parameters
int_time = 1000; %integration time in us normal 250
scans = 30; %scans to average
enable = 1; % enable signal
spectrometerIndex = 0; % Spectrometer index to use (first spectrometer by
    default).
channelIndex = 0; % Channel index to use (first channel by default).

%% Set the parameters
invoke(flame, 'setIntegrationTime', spectrometerIndex, channelIndex,
    int_time);
invoke(flame, 'setCorrectForDetectorNonlinearity', spectrometerIndex,
    channelIndex, enable);
invoke(flame, 'setCorrectForElectricalDark', spectrometerIndex,
    channelIndex, enable);
invoke(flame, 'setScansToAverage', spectrometerIndex, channelIndex, scans)
    ;
writeline(s,'o');

%%
[wavelength, backgroundIntensity] = getSpectrumBlue(s,flame,'o');
[wavelengthblue, intensityblue] = getSpectrumBlue(s,flame,'b');
[wavelengthUV, intensityUV] = getSpectrumBlue(s,flame,'u');
writeline(s,'o');

outputArrayBlue = [wavelengthblue (intensityblue-backgroundIntensity)];
outputArrayUv = [wavelengthUV (intensityUV-backgroundIntensity)];

writematrix(outputArrayBlue,strcat(ph_value,sensor,'_blue'));
writematrix(outputArrayUv,strcat(ph_value,sensor,'_uv'));
% % writematrix(outputArrayBlue,strcat(ph_value,'_blue'));
% writematrix(outputArrayUv,strcat(ph_value,'_uv'));

%% Plot Data
plot(outputArrayBlue(:,1),outputArrayBlue(:,2));
hold on;
plot(outputArrayUv(:,1),outputArrayUv(:,2));

%% Disconnect from spectrometer and LED controller

clear s;
disconnect(flame);
delete (flame);
delete(instrfindall);
```

A.5. Plotting data obtained with MATLAB script

```
folder = '611_6';

fileNameblue = '*blue*';
fileNameUv = '*uv*';
wavelength = 520;
wavelength_uv = 435;
blue = dir(fullfile(folder,fileNameblue));
uv = dir(fullfile(folder,fileNameUv));
peaksblue = zeros(1,length(uv));
peaksUV_450 = zeros(1,length(uv));
pH_values = [6.2 6.6 7 7.4 7.8 8.2];
newpH_values = [6.2 6.4 6.6 6.8 7 7.2 7.4 7.6 7.8 8.0 8.2];


for i = 1:length(ratioblue)
    peaksblue(i) = findWavelength_max(wavelength,table2array(readtable(
        fullfile(folder,blue(i).name))));
    peaksUV_450(i) = findWavelength_max(wavelength_uv,table2array(
        readtable(fullfile(folder,uv(i).name))));
end

ratio = peaksblue./peaksUV_450;


x0=10;
y0=10;
width=750;
height=500;
set(gcf,'position',[x0,y0,width,height])
ratio_norm = ratio./max(ratio);

plot(newpH_values,ratio_norm, 'LineWidth',1 );
grid on;
hold on;
xlabel("pH");
ylabel("Normalised intensity ratio");
title("Ratiometric measuremnent with whole sensor system");
```

A.6. Response time measurement script

```
1
2  % close all;
3  sensor = '_1';
4  ph_value = '8_2';
5  %% connect to spectrometer and LED controller
6  port = 'COM20';
7  s = serialport(port,115200);
8  flame = icdevice('OceanOptics_OmniDriver.mdd');
9  connect(flame);
10
11
12 %% initialize spectrum parameters
13 int_time = 1000; %integration time in us normal 250
14 scans = 200; %scans to average
15 enable = 1; % enable signal
16 spectrometerIndex = 0; % Spectrometer index to use (first spectrometer by
       default).
17 channelIndex = 0; % Channel index to use (first channel by default).
18
19 %% Set the parameters
20 invoke(flame, 'setIntegrationTime', spectrometerIndex, channelIndex,
       int_time);
21 invoke(flame, 'setCorrectForDetectorNonlinearity', spectrometerIndex,
       channelIndex, enable);
22 invoke(flame, 'setCorrectForElectricalDark', spectrometerIndex,
       channelIndex, enable);
23 invoke(flame, 'setScansToAverage', spectrometerIndex, channelIndex, scans)
       ;
24 writeline(s,'o');
25 N = 400;
26
27 peaksblue = linspace(1,2,1000);
28 peaksUV_450 = linspace(1,2,1000);
29 ratio = zeros(1,N);
30 wavelength_blue = 520;
31 wavelength_UV = 435;
32
33 Tstart = tic;
34 for i = 1:N
35
36 [wavelength, backgroundIntensity] = getSpectrumBlue(s,flame,'o');
37 [wavelengthblue, intensityblue] = getSpectrumBlue(s,flame,'b');
38 [wavelengthUV, intensityUV] = getSpectrumBlue(s,flame,'u');
39 writeline(s,'o');
40
41 outputArrayBlue = [wavelengthblue (intensityblue-backgroundIntensity)];
42 outputArrayUv = [wavelengthUV (intensityUV-backgroundIntensity)];
43 peaksblue = findWavelength(wavelength_blue,outputArrayBlue); %important
44 peaksUV_450 = findWavelength(wavelength_UV,outputArrayUv);
45 ratio(i) = peaksblue./peaksUV_450;
46 % writematrix(outputArrayBlue,strcat(ph_value,sensor,'_blue'));
47 % writematrix(outputArrayUv,strcat(ph_value,sensor,'_uv'));
48 % % writematrix(outputArrayBlue,strcat(ph_value,'_blue'));
49 % writematrix(outputArrayUv,strcat(ph_value,'_uv'));
```

```
50 pause(1);
51 i
52 end
53 Tstop = toc(Tstart);
54 %% Disconnect from spectrometer and LED controller
55
56 clear s;
57 disconnect(flame);
58 delete (flame);
59 delete(instrfindall);
```

A.7. Script to plot the Response time curve

```
1
2  load('703_response5.mat');
3
4  t = linspace(1,Tstop,length(ratio));
5  part = 200;
6  x0=10;
7  y0=10;
8  width=400;
9  height=300;
10 set(gcf,'position',[x0,y0,width,height])
11 plot(t(1:part),ratio(1:part)./max(ratio),"LineWidth",1);
12 % plot(t(:),ratio(:)./max(ratio),"LineWidth",1);
13 xline(10,'--r',"LineWidth",0.5);
14 xline(43, '--b', 't = 30 s', 'LineWidth', 0.5, 'LabelVerticalAlignment', '
       top');
15 yline(0.8, '--b', '8.2', 'LineWidth', 0.5, 'LabelHorizontalAlignment', '
       right')
16 yline(0.35, '--r', '6.2', 'LineWidth', 0.5, 'LabelHorizontalAlignment', '
       left')
17 grid on;
18 xlabel("Time [s]");
19 ylabel("Normalised intensity ratio");
20 title("Response time measurement");
```

B

Fabrication protocols

B.1. Protocol producing HPTS loaded Microbeads

Materials needed:

- Glass beaker 150 mL
- Glass beaker 50 mL
- DM water 110 mL
- Amberchrom microbeads 1g
- HPTS 35mg
- Magnetic stirrer
- Pipet
- Precision scale
- Plastic storage container

Method:

Step 1: Produce HPTS solutions

1. Prepare 100 mL of DM water
2. Weigh 35 mg of HPTS on the precision scale
3. Mix together using the magnetic stirrer

Step 2: Produce microbeads solution

1. Prepare 10mL of DM water
2. Weigh 10g of microbeads on the precision scale
3. Mix together using the magnetic stirrer

Step 3: Mix HPTS and microbeads

1. Pour the microbeads solution into the HPTS solution
2. Mix together using the magnetic mixer for one day
3. Store in plastic container for further use.

Step 4: Extract HPTS loaded microbeads

1. Extract the water from the solution leaving only the microbeads in the glass beaker
2. Rinse the microbeads two times to ensure all unbounded HPTS is flushed out
3. Store the microbeads in a plastic container for further use.

B.2. Production Hydrogel and sensor layer

Materials needed:

- Glass beaker 50 mL
- DM water 1 mL
- Hydromed hydrogel 1g
- Ethanol 9 mL
- Precision scale
- Magnetic stirrer
- Pipet
- Plastic storage container
- Glass slides
- HPTS loaded microbeads 3.5g

Method:

Step 1: produce hydrogel

1. Weigh 1g of Hydromed hydrogel on precision scale
2. Prepare 9 mL ethanol and 1 mL of DM water in the glass beaker
3. Put the hydrogel in the ethanol solution and stir for 6h until fully dissolved.

Step 2: Mix hydrogel and HPTS loaded microbeads

1. Weigh 3.5g of HPTS loaded microbeads on the precision scale
2. Put the HPTS loaded microbeads in the hydrogel solution and stir for 1h
3. Deposit the hydrogel mixture on glass slides using a pipet

B.3. Fabrication pH buffer solutions